Functional Roles of Charged Amino Acid Residues on the Wall of the Cytoplasmic Pore of Kir2.1

Yuichiro Fujiwara[1] and Yoshihiro Kubo[1,2,3]

[1]Division of Biophysics and Neurobiology, Department of Molecular Physiology, National Institute for Physiological Sciences, Aichi 444-8585, Japan

[2]COE Program for Brain Integration and its Disorders, Tokyo Medical and Dental University Graduate School and Faculty of Medicine, Tokyo 113-8519, Japan

[3]SORST, Japan Science and Technology Corporation, Saitama 332-0012, Japan

It is known that rectification of currents through the inward rectifier K^+ channel (Kir) is mainly due to blockade of the outward current by cytoplasmic Mg^{2+} and polyamines. Analyses of the crystal structure of the cytoplasmic region of Kir2.1 have revealed the presence of both negatively (E224, D255, D259, and E299) and positively (R228 and R260) charged residues on the wall of the cytoplasmic pore of Kir2.1, but the detail is not known about the contribution of these charged residues, the positive charges in particular, to the inward rectification. We therefore analyzed the functional significance of these charged amino acids using single/double point mutants in order to better understand the structure-based mechanism underlying inward rectification of Kir2.1 currents. As a first step, we used two-electrode voltage clamp to examine inward rectification in systematically prepared mutants in which one or two negatively or positively charged amino acids were neutralized by substitution. We found that the intensity of the inward rectification tended to be determined by the net negative charge within the cytoplasmic pore. We then used inside-out excised patch clamp recording to analyze the effect of the mutations on blockade by intracellular blockers and on K^+ permeation. We observed that a decrease in the net negative charge within the cytoplasmic pore reduced both the susceptibility of the channel to blockade by Mg^{2+} or spermine and the voltage dependence of the blockade. It also reduced K^+ permeation; i.e., it decreased single channel conductance, increased open-channel noise, and strengthened the intrinsic inward rectification in the total absence of cytoplasmic blockers. Taken together, these data suggest that the negatively charged cytoplasmic pore of Kir electrostatically gathers cations such as Mg^{2+}, spermine, and K^+ so that the transmembrane pore is sufficiently filled with K^+ ions, which enables strong voltage-dependent blockade with adequate outward K^+ conductance.

The Journal of General Physiology

INTRODUCTION

Inward rectification of the current through the inwardly rectifying K^+ channel (Kir) is reportedly due to blockade by cytoplasmic Mg^{2+} (Matsuda et al., 1987; Vandenberg, 1987; Matsuda, 1988) and polyamines (Ficker et al., 1994; Lopatin et al., 1994; Fakler et al., 1995; Ishihara et al., 1996; Nichols and Lopatin, 1997). The strong voltage dependence and high susceptibility to blockade of Kir plays a key role in organizing I_{K1} within the cardiac action potential (Luo and Rudy, 1994; Matsuoka et al., 2003). After the isolation of Kir1.1 (Ho et al., 1993) and Kir2.1 cDNA (Kubo et al., 1993a), the structural elements that determine the properties of inward rectification were identified using mutagenesis. It was first found that D172, located in the second transmembrane region of Kir2.1, was an amino acid residue shown to contribute to inward rectification: a D172N mutant had reduced susceptibility to blockade by both cytoplasmic polyamines and $Mg^{2+}{}_i$ (Lu and MacKinnon, 1994; Stanfield et al., 1994; Wible et al., 1994), and D172 was thought to make a strong energetic contribution to the binding of the blockers. Another amino acid residue, S165, also in the second transmembrane region, just below the GYG selectivity filter, has been shown to be important for blockade by $Mg^{2+}{}_i$, but not by polyamines (Fujiwara and Kubo, 2002). Thus, it appears that the cytoplasmic blockers plug the permeation pathway at sites deep within the transmembrane pore, below the selectivity filter. On another aspect, E224 and E299, located outside the transmembrane region, appear to play different roles in inward rectification. Both E224G and E299S mutants reportedly show reduced susceptibility to blockade by cytoplasmic blockers (Taglialatela et al., 1995; Yang et al., 1995; Kubo and Murata, 2001), and based on analysis of the electrophysiological properties of E224G, E299S, and E224G/E299S, it was suggested that these residues foster blockade by mediating increases in the local spermine concentration (Kubo and Murata, 2001). Xie et al. (2002, 2003) also analyzed the

Correspondence to Yuichiro Fujiwara or Yoshihiro Kubo: yuichiro@nips.ac.jp or ykubo@nips.ac.jp

The online version of this article contains supplemental material.

Abbreviations used in this paper: EGFP, enhanced green fluorescent protein; Kir, inwardly rectifying K^+ channel.

functional significances of E224 and E299 using synthesized polyamines of various length and suggested that spermine binds to these residues, thereby contributing to a surface charge screening effect. This suggests that E224 and E299 coordinate the intermediate binding of spermine without actually occluding K^+ permeation, which in turn increases the susceptibility to spermine blockade at a deeper site, near D172. On the other hand, Guo and Lu (2003) reported that polyamines block the permeation pathway at the level of E224 and E299. Thus the functional significance of these amino acid residues within thes cytoplasmic pore has not yet been conclusively defined.

In recent years, the crystal structures of several Kir channels have been solved. The structure of the cytoplasmic region of Kir3.1 was determined by Nishida and MacKinnon (2002), and the structure of bacterial Kir channel was determined by Kuo et al. (2003). In addition, Pegan et al. (2005) recently succeeded in resolving the structure of the cytoplasmic region of Kir2.1. These crystal structures have revealed that Kir has a long permeation pathway comprised of transmembrane and cytoplasmic pore regions. As expected, E224 and E299 are located on the wall of the cytoplasmic pore along with two other negatively charged residues, D259 and D255 (Fig. 1), and Pegan et al. (2005) reported that this di-aspartate cluster (D259 and D255) is also important in determining the extent of inward rectification. Not expected was the finding that there were also positively charged residues (R228 and R260) on the wall, the functional significance of which is unknown.

With that as background, our aim in the present study was to clarify the functional significance of the charged amino acid residues on the wall of the cytoplasmic pore of Kir2.1 and to better understand the structure-based mechanism underlying inward rectification of Kir2.1 currents. To that end, we made single and double point mutants by substituting the aforementioned charged amino acids and systematically analyzed the inward rectification properties of the resultant channels. Using two-electrode voltage clamp, we analyzed the intensity of inward rectification of currents through the mutant channels, as well as the activation of the inward and the decay of the outward currents. Using inside-out patch clamp recording, we analyzed the mutants' susceptibility to cytoplasmic blockers and their voltage dependence. As the characteristic properties of the inward rectification of Kir channel currents are reportedly linked to the permeant K^+ ions themselves (Hagiwara and Takahashi, 1974; Hagiwara and Yoshii, 1979; Oliver et al., 1998; Pearson and Nichols, 1998; Spassova and Lu, 1998), we also analyzed the permeation properties of the mutants; the single channel properties, and the intrinsic inward rectification in the total absence of the blockers.

MATERIALS AND METHODS

In Vitro Mutagenesis

The single point mutants were made with a QuickChange site-directed mutagenesis kit (Stratagene) using mutated oligonucleotide DNA primers and wild-type (WT) Kir2.1 cDNA (Fujiwara and Kubo, 2002). The introduction of each mutation was confirmed by sequencing with a BigDye Terminator Sequencing Kit (Applied Biosystems) and an automatic DNA sequencer (ABI type 310). The electrophysiological properties of two independent mutant clones were confirmed to be identical. Double-point mutants were made using single-point mutants as templates; triple mutants were prepared using double-point mutants.

Two-electrode Voltage Clamp Recordings in *Xenopus* Oocytes

Xenopus oocytes were collected from frogs anaesthetized in water containing 0.15% tricaine; after the final collection, the frogs were killed by decapitation. Isolated oocytes were treated with collagenase (2 mg/ml, type 1, Sigma-Aldrich) and then injected with ~50 nl of cRNA solution prepared from linearized plasmid DNA using an RNA transcription kit (Stratagene), after which they were incubated for 2–4 d at 17°C in frog Ringer solution supplemented with 20 mM KCl (Kubo et al., 1993a). All experiments were conducted in accordance with the guidelines of the Animal Care Committees of National Institute for Physiological Sciences.

Macroscopic currents were recorded using two-electrode voltage clamp with a bath-clamp amplifier (OC-725C, Warner Co.). Stimulation and data acquisition and analysis were done on a Pentium-based computer using Digidata 1322A and pCLAMP software (Axon Instruments, Inc.). Intracellular glass microelectrodes were filled with 3 M potassium acetate with 10 mM KCl (pH 7.2). The microelectrode resistances ranged from 0.1 to 0.3 MΩ. Two Ag-AgCl pellets (Warner Co.) were used to pass the bath current and sense the bath voltage. The voltage-sensing electrode was placed near the oocyte (~2 mm away), on the same side as the voltage-recording microelectrode. The bath current-passing pellet and the current injection microelectrode were placed on the other side. Under these conditions, the series resistance between the oocyte surface and the bath voltage-sensing pellet was ~200 Ω (Sabirov et al., 1997). As the measured current at the most hyperpolarized potential was 25 μA in the largest case, and was mainly <20 μA, the voltage-clamp error due to this series resistance was estimated to be no more than 5 mV and mostly <4 mV. This error, which was not compensated in the experiments, did not change the conclusions drawn from the comparison of WT and mutant channels.

For the data in Figs. 2–4 and Tables I and II, the recording bath solution contained 8 mM KCl, 80 mM NMDG, 70 mM HCl, 3 mM $MgCl_2$, 5 mM HEPES, and 2 mM KOH (pH 7.4). All recordings in this work were performed while the preparation was superfused with bath solution (7 ml/min) at room temperature (20–23°C). By assuming an intracellular K^+ concentration (K_i) of 80 mM, the E_K was calculated to be −52 mV; however, the exact values of K_i and E_K for each oocyte are unknown. The E_Ks used for calculation of the chord conductance (Fig. 2) were therefore adjusted to yield continuous G-V plots. The adjusted E_Ks ranged from −54 to −49 mV.

Data from the same batch of oocytes were used for comparison of phenotypes (Figs. 2–4, Fig. 9 A, and Tables I and II) because properties such as inward rectification and blocking speed differ significantly from batch to batch. Similar tendencies were reproducibly observed in five batches of oocytes.

Expression in HEK293T Cells

The cDNAs for WT and mutant Kir2.1 were subcloned into the pCXN2 expression vector (Niwa et al., 1991). The plasmid DNA

was then cotransfected into HEK293T cells (human embryonic kidney cell line) with a transfection marker, enhanced green fluorescent protein (CLONTECH Laboratories, Inc.; 1/15 the amount of plasmid DNA), using Lipofectamine Plus (GIBCO BRL), as instructed by the manufacturer. The cells were then cultured for 24 h in Dulbecco's modified Eagle's medium with 10% bovine calf serum. The transfectants were dissociated 12–15 h later by treatment with 0.025% trypsin in Ca^{2+}-, Mg^{2+}-free PBS and reseeded on coverslips at a relatively low density. The reseeding was done to obtain well-isolated cells and to facilitate successful GΩ seal formation. We confirmed previously that the trypsin treatment did not change the electrophysiological properties of the expressed channels (Kubo and Murata, 2001; Fujiwara and Kubo, 2002). Electrophysiological recordings were performed 7–24 h after reseeding, which corresponds to 18–35 h after transfection.

Macroscopic Current Recordings in HEK293T Cells

A coverslip with HEK293T cells was placed in a recording chamber containing bath solution (see below) on the stage of an inverted fluorescence microscope (IX70, Olympus), and the transfected cells were identified by the fluorescent signal from the cotransfected green fluorescent protein. Macroscopic currents were then recorded in the excised inside-out patch configuration using an Axopatch-1D amplifier. The resistance of the patch pipettes ranged from 1.0 to 1.5 MΩ. 60–80% of the voltage error due to the series resistance was compensated by a circuit in the amplifier. The high expression level achieved by the combination of HEK293T cells and the pCXN2 expression enabled macroscopic current recording using standard-sized patch pipettes. The recorded currents were low-pass filtered at 1 kHz by a circuit built into the amplifier and digitized at 5 kHz. In all experiments, the recording chamber was perfused with the bath solution at room temperature (20–23°C) during the recordings.

The pipette (extracellular side) and the bath (intracellular side) solution containing various concentrations of Mg^{2+} or spermine were prepared as described previously (Fujiwara and Kubo, 2002) with some modifications. We used KH_2PO_4 and K_2HPO_4 as pH buffers instead of HEPES because HEPES, or some accompanying impurity, reportedly blocks the outward current (Guo and Lu, 2000b, 2002). The pipette (extracellular side) solution contained 1.33 mM KCl, 120 mM NMDG, 102 mM HCl, 3 mM $MgCl_2$, 2.83 mM KH_2PO_4, 7.17 mM K_2HPO_4, and 1.5 mM KOH (pH 7.2) (Figs. 5–9). Mg^{2+}- and spermine-free bath solution contained 116.88 mM KCl, 2 mM EDTA, 2.83 mM KH_2PO_4, 7.17 mM K_2HPO_4, and 5.95 mM KOH (pH 7.2). The total K_o and K_i were ∼20 and 140 mM, respectively. In the experiment of Fig. 9, we used appropriate combinations of KH_2PO_4 and K_2HPO_4 as follows in the blockers-free bath solutions. They contained 9.4 mM and 0.6 mM (pH 8.0), 3.81 mM and 6.19 mM (pH 6.6), 1.92 mM and 8.08 mM (pH 6.2), and 0.85 mM and 9.15 mM (pH 5.8). The total K^+ concentration was adjusted to 140 mM (containing with 2 mM EDTA) using KCl and KOH. $MgCl_2$ was added to adjust the free Mg^{2+} concentration; the amount added was calculated using Sliders software (Chris Patton, Stanford University, http://www.stanford.edu/~cpatton/maxc.html). The amounts of added $MgCl_2$ and the (free Mg^{2+}) concentration were as follows: 1.06 mM (3.00 μM), 1.87 mM (30.5 μM), 2.28 mM (298 μM), 5 mM (3 mM), and 7 mM (5 mM) at pH 7.2; 38.7 μM (3.00 μM), 338 μM (30.0 μM), 1.59 mM (300 μM), 4.9 mM (3 mM), and 7 mM (5 mM) at pH 5.8. The acidic shift in pH caused by adding $MgCl_2$ was adjusted to pH 7.2 by applying KOH and KCl, and the total K^+ concentration was adjusted to 140 mM. Spermine (Sigma-Aldrich) was simply added to the solution just before the experi ments, and solutions containing spermine were used for up to 2 h. The concentration of added spermine is indicated in Fig. 6. The liquid junction potential between the pipette solution and the bath solution was ∼11 mV (Figs. 5–6 and Fig. 9 B); membrane potentials were corrected for this value off-line. In Fig. 8 and Fig. 9 C, the data were recorded using the Mg^{2+}- and spermine-free bath solution on both extracellular and intracellular sides.

The degree of rundown that occurred during the recordings used for determining I-V relationships was monitored by reapplying step pulses, and data with apparent rundown were discarded. For polyamine-free experiments, recordings were started after intensive perfusion of the bath (intracellular side) solution for 10–15 min to completely wash out endogenous polyamines.

Single-channel Recordings in *Xenopus* Oocytes

For single-channel recordings, the vitelline membrane was peeled off by bathing the oocytes in a hyperosmolar solution for 5–10 min (Kubo et al., 1993a). The patch pipettes were prepared from borosilicate glass (Warner Instruments) using a P-97 horizontal puller (Sutter) and a fire polisher (Narishige). Pipette resistance ranged from 1 to 2 MΩ. Recordings were made in the cell-attached configuration using an AxoPatch 1D amplifier (Axon Instruments, Inc.). The recorded currents were low pass filtered at 1 kHz using a Bessel filter built into the amplifier and digitized at 5 kHz. The pipette (extracellular) and bath solutions contained 116.88 mM KCl, 2 mM EDTA, 2.83 mM KH_2PO_4, 7.17 mM K_2HPO_4, and 5.95 mM KOH (pH 7.2).

Leak Subtraction

Leak subtraction was not done for the data summarized in Figs. 2–6 and Fig. 9 (A and B). But when assessing the intensity of inward rectification, it is critical to avoid contamination of the leak component. We therefore avoided setting $E_K = 0$ mV because that would be difficult to discriminate between the outward Kir currents and the leak component. We instead used mixture of K^+ and NMDG in the extracellular solution to set E_K at, for example, −50 mV. We then carefully monitored the reversal potential during the recordings and judged whether the leak level was ignorable by confirming that the reversal potential remained at the expected level. Only data that satisfied these criteria were used for analysis. Because we recorded intrinsic rectification using symmetrical recording solutions ($E_K = 0$ mV) in the experiments summarized in Fig. 8 and Fig. 9 C, leak subtraction was necessary. To do so, we added 20 mM Mg^{2+} to the bath intracellular solution to cause the Kir2.1 channels to rundown; and then after 5 min, a background current was recorded as a template for leak subtraction.

Data Analysis

Data were analyzed using Clampfit 8 and 9 (Axon Instruments, Inc.), Igor Pro (WaveMetrics, Inc.), and KyPlot (KyensLab, Inc.) software. The means of two groups were compared using Student's *t* test, while pairs of means among three or more groups were compared using Tukey's test, and the difference among the means of multiple groups was tested using one-way ANOVA.

The susceptibility of WT and mutant channels to blockers was evaluated based on *K*d values, which were calculated by fitting the data with Hill's equation. The voltage dependence of the blockade was analyzed using *K*d values obtained at various voltages using the following equation (Hille, 2001):

$$z\sigma = \log\frac{Kd_{(A)}}{Kd_{(B)}} \times \frac{2.303RT}{F\Delta E_{(A-B)}},$$

where R is the Gas constant, T is the absolute temperature, and F is Faraday's constant. In this study, the z values were 2 and 4 for the Mg^{2+} and spermine blockades, respectively, and σ was calculated by fitting voltage-*K*d plots with a linear line (Figs. 5, 6, and 9).

Single-channel conductance and the open-close event histogram were analyzed using Clampfit 9 (Axon Instruments, Inc.) and Igor Pro

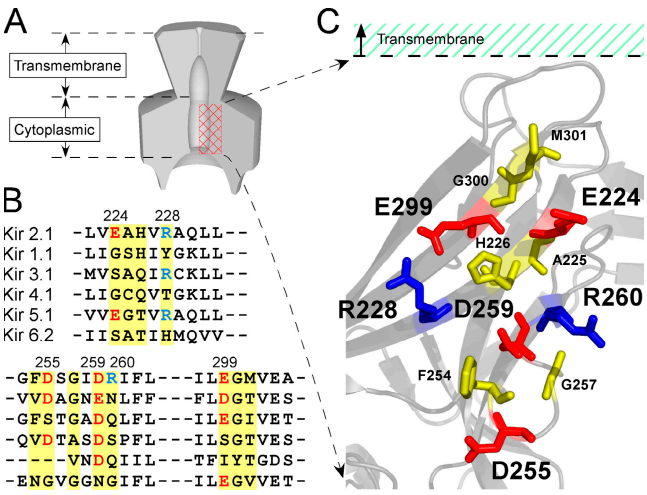

Figure 1. Structure of the cytoplasmic pore of Kir2.1. (A) Schematic drawing of the structure of Kir based on the crystal structures of Kir2.1, Kir3.1, and KirBac1.1 (Nishida and MacKinnon, 2002; Kuo et al., 2003; Pegan et al., 2005); note that the pore has both transmembrane and cytoplasmic regions. (B) Alignment of the amino acid sequences of Kir family proteins that form the wall of the cytoplasmic pore and the surrounding region. The original reports used for the alignment are as follows: Kir 2.1 (Kubo et al., 1993a), Kir1.1 (Ho et al., 1993), Kir 3.1 (Kubo et al., 1993b), Kir 4.1 (Bond et al., 1994; Takumi et al., 1995), Kir5.1 (Bond et al., 1994), Kir 6.2 (Inagaki et al., 1995). (C) Amino acids on the wall of the cytoplasmic pore of Kir2.1. Negatively charged residues (E224, D255, D259, and E299) are colored red, positively charged residues (R228 and R260) are colored blue, and other residues are colored yellow.

(WaveMetrics, Inc). Mean single channel conductance was calculated using the data in the event histogram (Fig. 7).

Detection of Cell Surface Expression

We analyzed the surface expression of nonfunctional mutants of Kir2.1 by detecting fluorescent signals attached to the channels under fluorescent microscope. Enhanced green fluorescent protein (EGFP)–tagged constructs of Kir2.1 WT, nonfunctional mutants, and ΔFCYENEV were made by PCR using primers that include EcoRI(5′) and BamHI(3′) sites. ΔFCYENEV is a deletion mutant of the trafficking motif (F_{374}CYENEV$_{380}$) (Ma et al., 2001; Stockklausner et al., 2001), and we used it as a negative control of surface expression. The EcoRI-Kir2.1-BamHI fragments were subcloned into the EGFP-N1 vector (CLONTECH Laboratories, Inc.) in frame. DNA sequences of the inserted fragments and the surrounding regions of all constructs were confirmed. L929 cells (mouse fibroblast cell line, RIKEN) were seeded onto poly-L-lysine–coated glass coverslips, where they were transiently transfected with the EGFP-tagged constructs using the Lipofectamine Plus (GIBCO BRL) according to the manufacturer's instructions. After 24 h, they were fixed by 4% paraformaldehyde and then rinsed three times with PBS. The coverslips were mounted on slide glasses using PermaFluor mounting medium (Shandon). Fluorescent images were acquired using an AxioCam cooled CCD camera (Carl Zeiss MicroImaging, Inc.). The images of the nonfunctional mutants were compared with images of positive (WT) and negative (ΔFCYENEV) controls.

Online Supplemental Material

In the online supplemental material (Fig. S1, available at http://www.jgp.org/cgi/content/full/jgp.200509434/DC1), we analyzed the surface expression of the nonfunctional mutants of Kir2.1. We detected fluorescent signals attached to the channels on the membrane surface of transfected L929 cells. The data showed that their cell surface expression levels were not significantly different from that of WT.

RESULTS

Charged Amino Acids on the Wall of the Inner Vestibule of Kir2.1

X-ray crystallographic analysis has shown that Kir has a long permeation pathway that extends through a cytoplasmic region and a transmembrane region; the scheme drawn in Fig. 1 A refers to the structures of Kir2.1, Kir3.1, and KirBac1.1 (Nishida and MacKinnon, 2002; Kuo et al., 2003; Pegan et al., 2005). Multiple alignment of the amino acid sequences of Kir family proteins are shown in Fig. 1 B; the amino acid residues facing the aqueous cavity of the cytoplasmic pore are colored yellow, negatively charged ones are colored red, and positively charged ones are colored blue. The surface of the permeation path through the cytoplasmic pore of one Kir2.1 subunit is illustrated in Fig. 1 C; the amino acid residues facing the aqueous pore are shown as sticks, the others as cartoons. Note that within the structure of Kir2.1, a cluster of hydrophilic residues lays between the hydrophobic residues F254 and M301. With the channel oriented as in the figure, the negatively charged residues E224 and E299 are located on the top of the cluster, and the positively charged residues R228 and R260 are below them, as is negatively charged D259. Negatively charged D255 is located at the bottom of the cytoplasmic pore, far below the transmembrane region.

E224 and E299 have been investigated previously using E224G and E299S mutants (Kubo and Murata, 2001; Guo and Lu, 2003; Xie et al., 2004). The function of the other charged residues (D255, D259, R228, and R260) have been also studied (Nishida and MacKinnon, 2002; Kuo et al., 2003; Pegan et al., 2005), but the detail has not been analyzed intensively regarding their contributions to the susceptibility to intracellular blockers, the single channel properties, and the intrinsic inward rectification. To address this issue, we systematically substituted these residues such that they were nearly unchanged in size, but were made electrostatically neutral (i.e., E→Q, D→N, and R→Q). As an initial step, we analyzed the electrophysiological properties of mutants using two-electrode voltage clamp with a *Xenopus* expression system.

Contribution of Charged Amino Acids to Inward Rectification

We examined the electrophysiological effects of neutralizing the charged residues within the cytoplasmic pore of Kir2.1 (Fig. 2 and Table I). Macroscopic

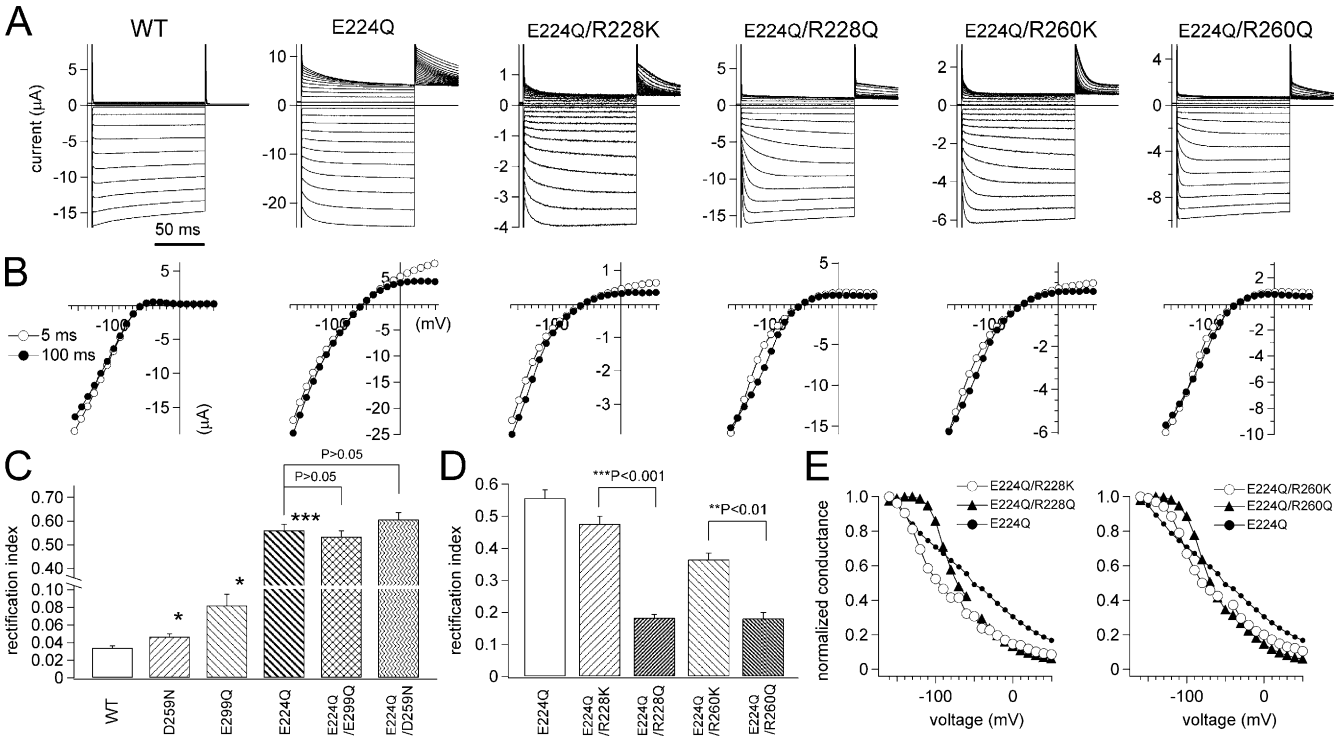

Figure 2. Comparison of macroscopic currents through WT Kir2.1 and mutants. (A) Macroscopic currents recorded using two-electrode voltage clamp with *Xenopus* oocytes in 10 mM K^+_o. The holding potential was −50 mV; step pulses from +50 to −160 mV were applied in 10-mV decrements. (B) Current–voltage (I-V) relationships for the data in A; values were measured 5 or 100 ms after the onset of each step pulse. (C and D) Comparison of the intensities of the inward rectification of currents through WT Kir2.1 and the mutants. The ratios of the current amplitudes measured 100 ms after the onset of step pulses to +50 and −100 mV were calculated as an index of the rectification intensity. Bars depict means ± SEM (n = 5–8) in C and means ± SEM (n = 3–5) in D. Mean values were compared statistically using Tukey's test (***, $P < 0.001$; **, $P < 0.01$; *, $P < 0.05$). (E) Representative G-V relationships for the macroscopic currents in which the indicated mutants were compared.

currents recorded in 10 mM K^+ are shown in Fig. 2 A, while the I-V relationships are shown in Fig. 2 B. As an index of the intensity of the inward rectification, the ratios of the current amplitudes at +50 and −100 mV, measured 100 ms after the onset of the step pulses were calculated (Fig. 2, C and D).

We first describe the effects of neutralizing the negative charges. Inward rectification was weakened in all of the single point mutants (E224Q, D259N, and E299Q) (Fig. 2 C and Table I, group 1), especially in E224Q, which showed a large outward current (Fig. 2 A). Addition of E299Q or D259N mutation to E224Q did not affect inward rectification remarkably. We also analyzed the functional significance of D255, located at the bottom in the cytoplasmic aqueous pore (Fig. 1 C) and found that D255N mutation had little effect on the intensity of inward rectification (Table I, group 2). Pegan et al. (2005) reported that both D259 and D255 were important for inward rectification. This discrepancy might reflect the difference in the mutants used: they used D255R, whereas we used D255N. These results suggest that negative charges (E224, E299, and to a minor extent D259) on the wall of the cytoplasmic pore are key determinants of the strength of the inward rectification of the currents through Kir2.1.

We next analyzed the effects of neutralizing the positive charges within the cytoplasmic pore of Kir2.1. Data obtained with R228Q, R260Q, and R228Q/R260Q using two-electrode voltage clamp are summarized in Table I, group 3. Although both R228Q and R260Q were highly expressible, no macroscopic currents through the R228Q/R260Q double mutant were observed. R228Q and R260Q currents showed strong inward rectification, and the difference from WT was subtle. We suspected that the significance of these positively charged residues was masked by the presence of adjacent negative charges, so we made the E224Q/R228Q and E224Q/R260Q double mutants and compared them with E224Q, E224Q/R228K, and E224Q/R260K (Fig. 2 and Table I, group 4). Introduction of the additional R228Q mutation substantially increased the intensity of the inward rectification of E224Q, whereas the R228K mutation had no clear effect (Fig. 2 C and Table I, group 4). Similar tendencies were observed with E224Q, E224Q/R260K, and E224Q/R260Q. To further examine the electrostatic effect of these residues, we also made two inversely charged single point mutations, R228E and R260E, but the latter carried no detectable current. R228E mutation strengthened the

TABLE I

Summarized Data on the Contribution of Charged Residues to the Intensity of Inward Rectification Obtained using Two-electrode Voltage Clamp

Group	Mutant	Inward rectification intensity	Statistical analysis
1	WT	0.034 ± 0.003 (n = 6)	control
	E224Q	0.560 ± 0.026 (n = 5)	***
	D259N	0.047 ± 0.003 (n = 6)	*
	E299Q	0.082 ± 0.013 (n = 5)	*
	E224Q/E299Q	0.534 ± 0.025 (n = 8)	***
	E224Q/D259N	0.606 ± 0.029 (n = 5)	***
	E299Q/D259N	ND	
	E224Q/E299Q/D259N	ND	
2	WT	0.044 ± 0.005 (n = 5)	control
	D255N	0.047 ± 0.007 (n = 5)	P > 0.05
	E224Q	0.668 ± 0.013 (n = 4)	control
	E224Q/D255N	0.604 ± 0.027 (n = 5)	P > 0.05
3	WT	0.040 ± 0.007 (n = 5)	control
	R228Q	0.082 ± 0.009 (n = 7)	*
	R260Q	0.074 ± 0.010 (n = 7)	P > 0.05
	R228Q/R260Q	ND	
4	E224Q	0.56 ± 0.03 (n = 4)	
	E224Q/R228K	0.48 ± 0.02 (n = 5)	***
	E224Q/R228Q	0.18 ± 0.01 (n = 4)	control
	E224Q/R260K	0.36 ± 0.02 (n = 3)	**
	E224Q/R260Q	0.18 ± 0.02 (n = 3)	control
5	E224Q	0.46 ± 0.02 (n = 5)	
	E224Q/R228Q	0.20 ± 0.01 (n = 4)	control
	E224Q/R228E	0.15 ± 0.01 (n = 4)	**
6	E299Q	0.096 ± 0.016 (n = 6)	control
	E299Q/R228Q	0.046 ± 0.006 (n = 6)	**
	E299Q/R260Q	ND	
	D259N	0.065 ± 0.008 (n = 5)	control
	D259N/R228Q	ND	
	E259N/R260Q	0.039 ± 0.003 (n = 6)	*
7	E224G	0.30 ± 0.02 (n = 5)	control
	E224G/R228Q	0.14 ± 0.01 (n = 6)	***
	E224G/R260Q	0.23 ± 0.03 (n = 5)	*
	E299S	0.40 ± 0.05 (n = 5)	control
	E299S/R228Q	0.12 ± 0.02 (n = 6)	***
	E299S/R260Q	0.36 ± 0.05 (n = 5)	P > 0.05
8	WT	0.036 ± 0.004 (n = 5)	control
	H226Q	0.046 ± 0.006 (n = 4)	P > 0.05
	H226K	0.099 ± 0.020 (n = 4)	**

For comparison of the phenotypes, mean values for WT and mutant channels were analyzed statistically using Tukey's test or Student's t test (***, P < 0.001; **, P < 0.01; *, P < 0.05). ND denotes channels that were expressed only poorly or not at all, and so could not be analyzed. Data from the same batch of oocytes were used for comparison of phenotypes.

intensity of the inward rectification of E224Q, and the effect was stronger than that seen with E224Q/R228Q (Table I, group 5).

At hyperpolarized potentials, these mutations also affected the G-V relationship (Fig. 2 E). The macroscopic channel conductance recorded using two-electrode voltage clamp was clearly influenced by introducing the E224Q mutation: it did not reach saturation, even at the most hyperpolarized potential recorded (−160 mV). The macroscopic conductance of E224Q/R228Q saturated at membrane potentials more hyperpolarized than −130 mV, while the G-V relationship of E224Q/R228K did not saturate at −160 mV, as was observed with E224Q (Fig. 2 E). These changes in the macroscopic conductance suggest that K^+ permeation and the unbinding of cytoplasmic blockers at hyperpolarized potentials were influenced by the neutralization of charged residues within the cytoplasmic pore of Kir2.1.

To further confirm the electrostatic effect of these residues, we also analyzed the effect of R→Q neutralized mutation on other background mutants: E299Q, D259N, E224G, or E229S (Table I, groups 6 and 7). Addition of an R228Q or an R260Q mutation also strengthened inward rectification of the backgrounds (Table I, groups 6 and 7). In some cases, the mutant channels carried no detectable current, even when

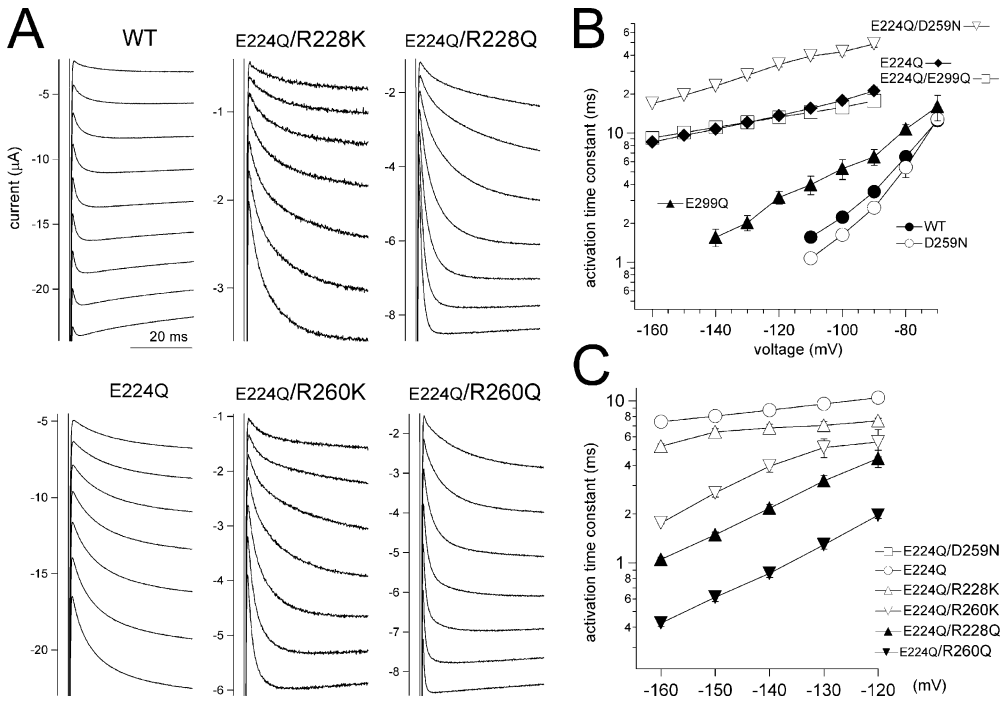

Figure 3. Comparison of the hyperpolarization-evoked activation kinetics in WT Kir2.1 and mutants. (A) Inward currents recorded using two-electrode voltage clamp with *Xenopus* oocytes at the indicated membrane voltages in 10 mM K^+_o. (B) The activation phases were fitted with a single exponential function, and the time constants of the fittings are plotted. The symbols used are as shown in the figure. Bars depict means ± SEM (n = 6–8). (C) Same as in B; in this case, data obtained from E224Q, E224Q/R228K, E224Q/R228Q, E224Q/R228K, or E224Q/R260K were compared. Bars depict means ± SEM (n = 3–4).

the oocytes were injected with highly concentrated (>20×) cRNA. There is a possibility that they are not expressed on the membrane surface. We therefore attached a tag of EGFP to the mutants and analyzed fluorescence signal on the membrane surface of transfected L929 cells. Fluorescent signals were clearly detected on the cell surface for WT-EGFP (positive control), while they were detected only from the cytoplasm for ΔFCYENEV-EGFP (negative control) (see Fig. S1, available at http://www.jgp.org/cgi/content/full/jgp.200509434/DC1). The signals of all nonfunctional mutants were clearly detected on the cell surface similarly to those of WT-EGFP (Fig. S1). These results suggest that the lack of function is not due to the problem of surface expression, implying that the role of the charged amino acid residues on K^+ permeation is critical. As all double mutants on the background of E224Q showed sufficient functional expression, we used, in this study, E224Q as a representative background mutant that showed weak inward rectification.

Contribution of Charged Amino Acids to Activation

The activation phases upon hyperpolarization of WT Kir2.1 and the mutants with neutralized charges were recorded in 10 mM K^+. The current traces obtained with WT at −70 to −150 mV, with E224Q, E224Q/R228K, E224Q/R228Q, E224Q/R260K, and E224Q/R260Q at −100 to −160 mV are shown in Fig. 3 A. The time constants obtained by fitting the data with a single exponential function are plotted in Fig. 3 (B and C); note that the inactivating component of the WT, E224Q/R228Q, and E224Q/R260Q currents (Fig. 3 A) was ignored in the fitting. At strongly hyperpolarized potentials, the activation phases of WT, D259N, and E299Q were too rapid to be separated precisely from the capacitative current, so they were not used for analysis. Upon introduction of E224Q mutation, the activation phases were noticeably slower (Fig. 3 A). We also analyzed neutralized mutants of the negative charges (E224, E299, and D259) and observed that they slow, with different extents, the activation of the inward current (Fig. 3 B and Table II, group 1). Addition of R228Q mutation to E224Q markedly accelerated activation of the inward current, whereas addition of R228K mutation had no significant effect (Fig. 3, A and C). Likewise, addition of R260Q mutation also markedly accelerated activation of the inward current, whereas addition of R260K mutation also had a significant but much smaller effect. It was also noteworthy that the voltage dependences of the time constants were strengthened by R228Q or R260Q mutation, contrary to the changes by neutralization of negative charges (Fig. 3, B and C). Taken together, these findings indicate that neutralization of positive charges on the wall of the

TABLE II

Summarized Data on the Contribution of the Charged Residues to the Activation of Inward Currents and Decay of Outward Currents Recorded Using Two-electrode Voltage Clamp

Group	Mutant	Activation speed			Decaying speed of the outward current				
		Single exp fitting (test −100 mV)	Statistical analysis		Fast component (pre −150 mV)	Statistical analysis		Slow component (pre −150 mV)	Statistical analysis
1	WT	2.23 ± 0.10 ms (n = 4)	control		ND (too fast)			ND (too fast)	
	E224Q	15.78 ± 0.49 ms (n = 6)	***	control	37.2 ± 2.2 ms (n = 6)	control		4526 ± 207 ms (n = 6)	control
	D259N	1.63 ± 0.14 ms (n = 4)	P > 0.05		16.5 ± 1.1 ms (n = 6)	*		93 ± 3 ms (n = 6)	***
	E299Q	5.29 ± 0.92 ms (n = 4)	**		1.8 ± 0.6 ms (n = 6)	**		28 ± 1 ms (n = 6)	***
	E224Q/E299Q	17.82 ± 0.97 ms (n = 6)	***	P > 0.05	72.9 ± 2.0 ms (n = 6)	**	***	6009 ± 175 ms (n = 6)	***
	E224Q/D259N	42.39 ± 2.99 ms (n = 6)	***	***	508.2 ± 16.6 ms (n = 5)	***		(−)	
		Single exp fitting (test −150 mV)	Statistical analysis		Fast component (pre −150 mV)	Statistical analysis		Slow component (pre −150 mV)	Statistical analysis
2	E224Q	8.05 ± 0.29 ms (n = 4)	control		52.4 ± 4.7 ms (n = 4)	control		4040 ± 170 ms (n = 4)	control
	E224Q/R228K	6.43 ± 0.31 ms (n = 4)	***	***	18.7 ± 0.5 ms (n = 5)	***	***	3054 ± 374 ms (n = 5)	**	***
	E224Q/R228Q	1.49 ± 0.06 ms (n = 4)	***		6.4 ± 0.7 ms (n = 6)	***		128 ± 11 ms (n = 6)	***	
	E224Q/R260K	2.70 ± 0.15 ms (n = 4)	***	***	5.6 ± 0.4 ms (n = 5)	***	*	1208 ± 116 ms (n = 5)	***	***
	E224Q/R260Q	0.61 ± 0.04 ms (n = 3)	***		2.1 ± 0.4 ms (n = 6)	***		52 ± 3 ms (n = 7)	***	

Mean values were compared statistically between WT and mutant channels using Tukey's test or Student's t test (***, P < 0.001; **, P < 0.01; *, P < 0.05). ND denotes phenotypes that were too fast to be analyzed; (−), not detectable.

cytoplasmic pore of Kir2.1 accelerated the activation of the inward current.

Contribution of Charged Amino Acids to the Decay of the Outward Current

We next analyzed the time courses of the tail currents at +50 mV after depolarization from various prepotentials. In Fig. 4 A, recordings of the outward currents are shown using a magnification scale normalized by the amplitude of the inward current at −120 mV. None of the currents could be fitted with a single exponential function. With the exception of the current through E224Q/D259N, they could be fitted with a double-exponential function, and representative time constants are plotted in Fig. 4 (B and C). The decay of the outward current through WT Kir2.1 was too fast to be analyzed separately from the capacitative current. By contrast, much larger in amplitude and slowly declining tail currents were observed with E224Q (Fig. 4, A and B). We also analyzed neutralized mutants of other negative charges (E299 and D259) and observed that they all slow the decay of the outward current (Fig. 4 B and Table II, group 1). The tail currents carried by E224Q/R228Q and E224Q/R260Q were smaller in amplitude and declined faster than those through E224Q (Fig. 4, A and C), while the currents through E224Q/R228K and E224Q/R260K were similar to those through E224Q (Fig. 4, A and C). It was also noteworthy that the tail current amplitudes increased after prepulses of strong hyperpolarized potentials in some mutants, apparently in E224Q, E224Q/R228K, and E224Q/R260K (Fig. 4 A). One possible interpretation about these phenomena is that these may be caused by the increase of the release of polyamines from the intermediate binding site in the cytoplasmic pore level when strong hyperpolarization is applied to these mutants (Kubo and Murata, 2001); and therefore current amplitudes would increase extra.

Contribution of Charged Residues to Blockade by Mg^{2+}

Given that inward rectification of Kir is caused by blockade of the permeation pathway by cytoplasmic Mg^{2+} or polyamines, we next determined how the susceptibility to blockade by these inhibitors is affected by mutation. The analysis summarized below was performed using WT Kir2.1 and R228Q, D259N, E224Q, E224Q/R228Q, and E224Q/D259N as representative mutants.

Macroscopic currents were recorded from inside-out membrane patches excised from HEK293T cells expressing WT or mutant Kir2.1 (Fig. 5); cells were held at −50 mV, and 500-ms test pulses from +70 to −120 mV were applied in 10-mV decrements. Representative

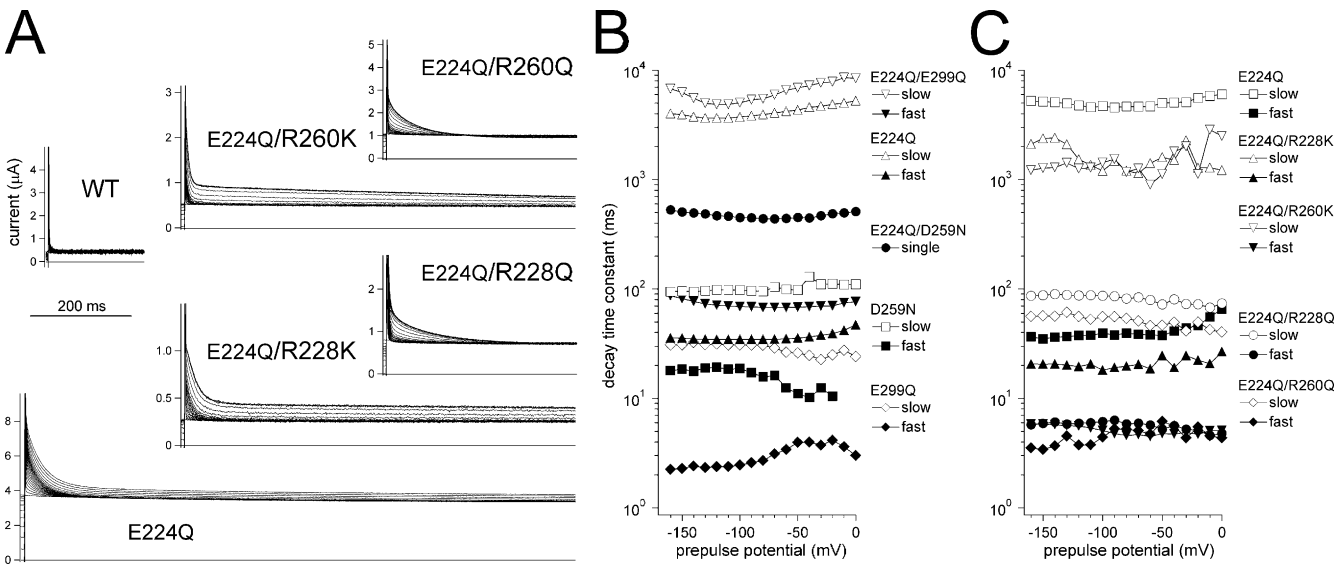

Figure 4. Comparison of the outward tail currents through WT Kir2.1 and mutants. All channels were expressed in *Xenopus* oocytes. (A) Outward currents recorded using two-electrode voltage clamp with *Xenopus* oocytes at +50 mV after depolarization from various potentials ranging from +50 to −160 mV. K^+_o was 10 mM. (B) The data obtained with E224Q, D259N, E299Q, and E224Q/E299Q were fitted with a two exponential function, while those obtained with E224Q/D259N were fitted with a single exponential function; the time constants are plotted. The bottom axis indicates the voltage of the preceding step pulses. The symbols used are as indicated in the figure. Representative data were plotted for each channel. (C) Same as in B; in this case, data obtained with E224Q, E224Q/R228K, E224Q/R228Q, E224Q/R228K, or E224Q/R260K were compared.

series of recordings made in the nominal absence of polyamines and in the presence of various concentrations of free Mg^{2+}_i (calculated as described in MATERIALS AND METHODS) are shown in Fig. 5. In the absence of polyamines and Mg^{2+}_i, the I-V relationships of WT and the mutants were not linear under these experimental conditions; for example, the I-V relationship for WT showed outward rectification consistent with the GHK equation, and that of E224Q showed intrinsic inward rectification.

At depolarized potentials, the outward current through WT was blocked almost instantaneously, even by low concentrations of Mg^{2+}_i (3 μM), while D259N currents were blocked more slowly by 3 μM Mg^{2+}_i (Fig. 5 A), suggesting that D259N was slightly less susceptible to blockade by Mg^{2+}_i than WT. This slow blockade of outward currents by Mg^{2+}_i was also observed with the other mutants. With E224Q, for example, a very slow blockade was observed in the presence of 300 μM Mg^{2+}_i; this blockade was accelerated by the introduction of an R228Q mutation (Fig. 5 A), and was slowed by introduction of a D259N mutation (current traces not shown).

We then analyzed the dose–block relationship by measuring the macroscopic conductances recorded from a single patch in a series of Mg^{2+}_i concentrations; data showing apparent rundown were discarded. The normalized dose–block relationships for currents measured 500 ms after the onset of the step pulses are plotted in Fig. 5 B and fitted with Hill's equation; the *K*d values (n = 3) obtained at each voltage were well fitted by a linear function as shown in Fig. 5 C. The voltage dependence of the *K*d values varied among mutants (Fig. 5, B and C), but were always linearly correlated. The means calculated from the fitted lines in Fig. 5 C are shown in Fig. 5 D, and the zσ values (calculated as described in MATERIALS AND METHODS) are shown in Fig. 5 E. Both the *K*d and the voltage dependence of the block by Mg^{2+}_i were affected by mutation. The *K*d value for the blockade of D259N at +70 mV was slightly larger than that for WT, and that for E224Q was much larger (Fig. 5, D and E). The voltage dependence of the blockade of D259N was slightly less steep than that of WT, and that of E224Q was much less steep (Fig. 5, D and E). These changes seen with E224Q were diminished by the introduction of a R228Q mutation, whereas they were enhanced by the introduction of a D259N mutation (Fig. 5, D and E). The Hill coefficients were changed significantly by the mutations and did not show significant correlations with the voltage (Fig. 5 F).

Contribution of Charged Residues to Blockade by Spermine

We next determined how the susceptibility to blockade by intracellular spermine was affected by the mutations. Macroscopic currents were recorded from inside-out membrane patches excised from HEK293T cells expressing WT or mutant Kir2.1 using 3-s step pulses. Representative series of recordings showing spermine blockade in the absence of Mg^{2+}_i are shown in Fig. 6. Outward currents through WT and D259N were blocked

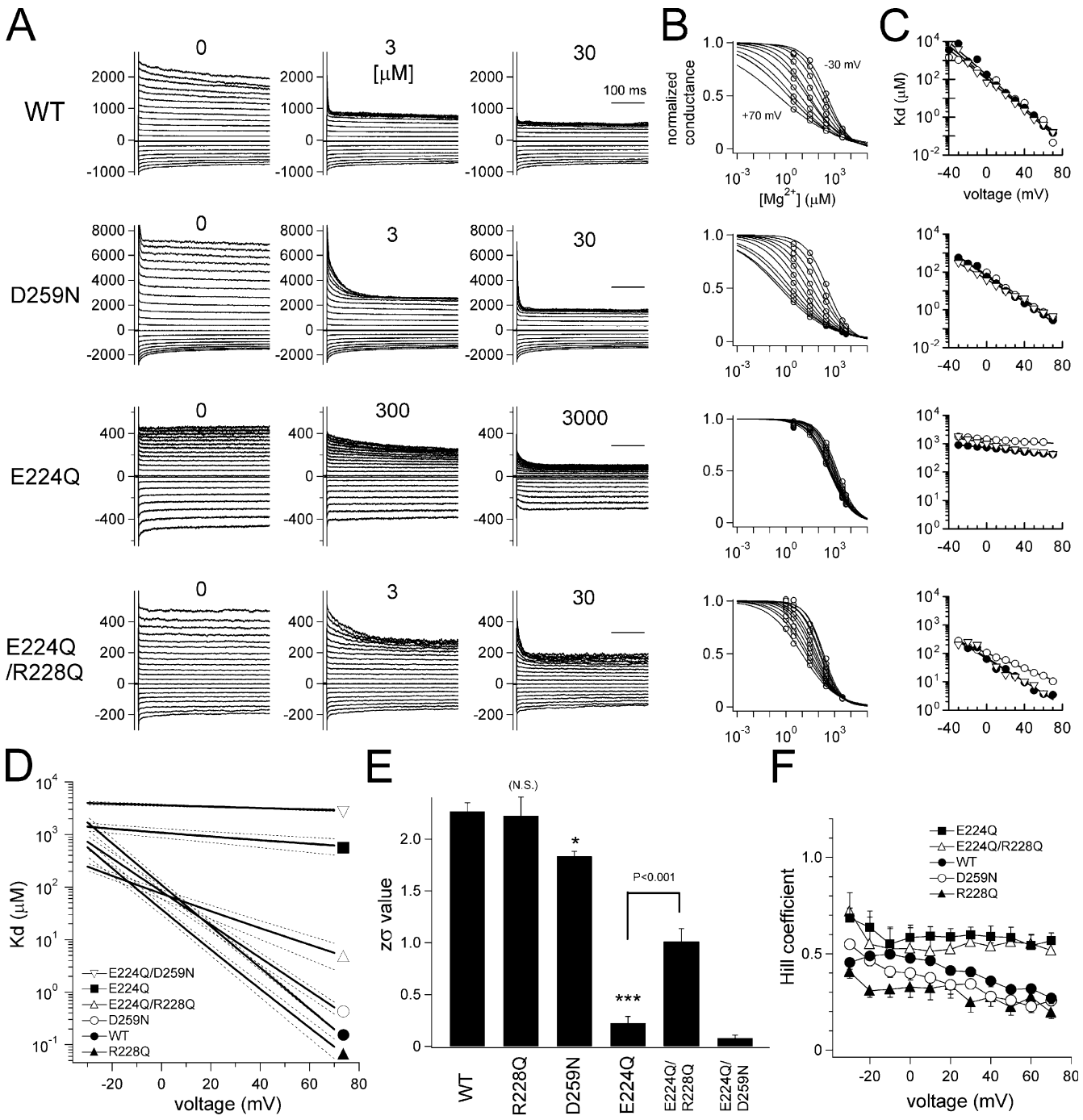

Figure 5. Comparison of the susceptibility of macroscopic currents through WT Kir2.1 and mutants to blockade by intracellular Mg^{2+}. (A) Macroscopic currents recorded in the presence of the indicated concentrations of $Mg^{2+}{}_i$ from excised patches of HEK293T cells expressing WT Kir2.1 or mutants. The concentrations of $Mg^{2+}{}_i$ are shown on the top; note the difference in the concentration ranges used for WT and E224Q. $K^+{}_o$ in the pipette was 20 mM, and $K^+{}_i$ in the bath was 140 mM. The calculated E_K was −49 mV. The holding potential was −50 mV, and step pulses from +70 to −120 mV were applied in 10-mV decrements. (B) Normalized dose–block relationships derived from data in A; values were measured 500 ms after the onset of each step pulse. (C) Relationships between the *K*d and voltage for $Mg^{2+}{}_i$ blockade of outward K^+ currents. Data obtained from three patches were plotted for each channel, and each set was fitted with a line. (D) Relationships between the voltage and the mean of the fitted lines in C, and the dashed lines indicate SEMs. (E) Zd values of each channel calculated from the slopes of the lines in C. Mean values were compared statistically between WT and the mutants using Tukey's test (***, $P < 0.001$; *, $P < 0.05$; NS, $P > 0.05$); statistical comparison of the data obtained from E224Q and E224Q/R228Q is also shown. (F) Values of the Hill coefficient for each channel. Bars depict means ± SEM ($n = 3$). The symbols used are as indicated in the figure.

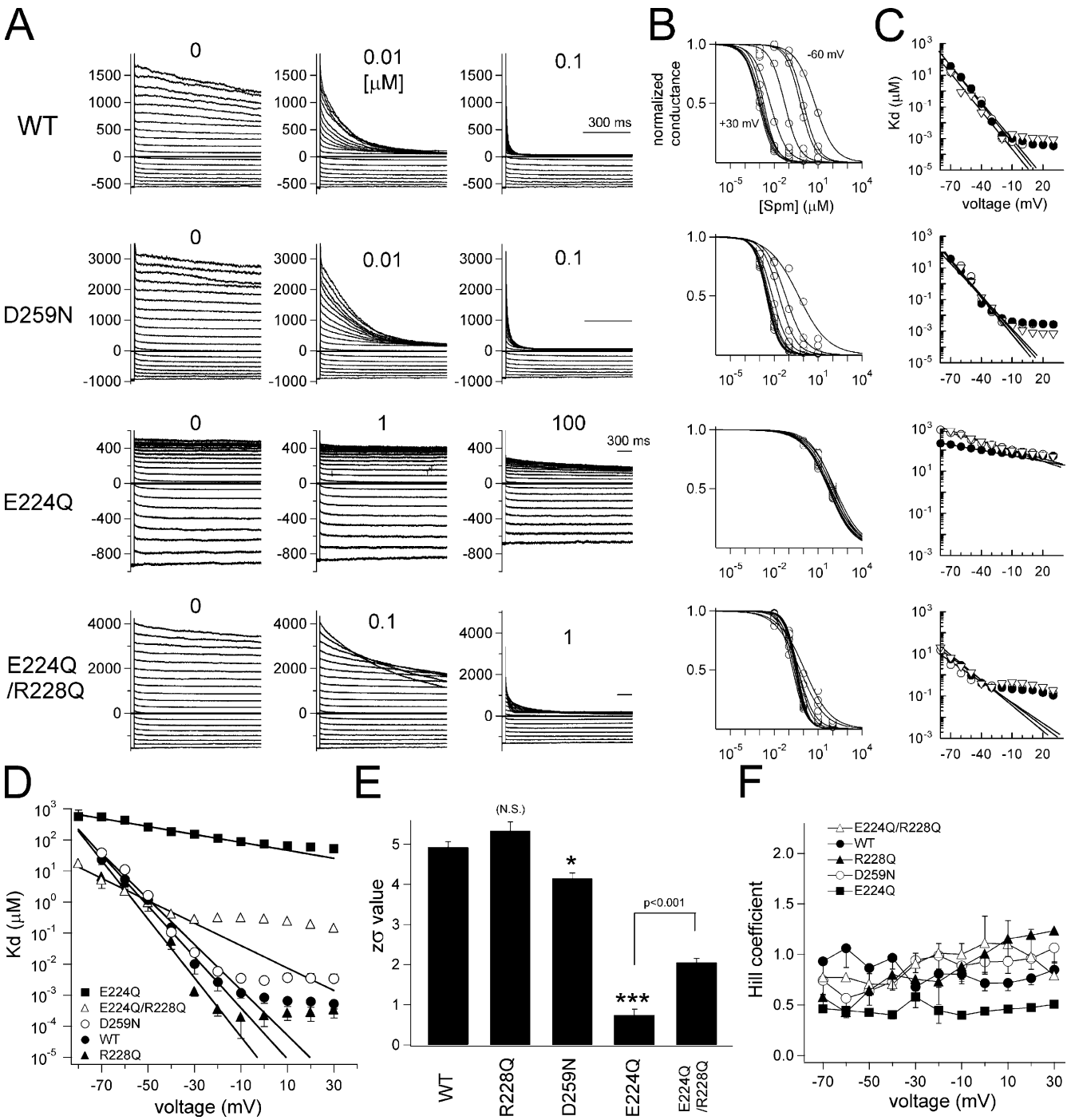

Figure 6. Comparison of the susceptibility of macroscopic currents through WT Kir2.1 and mutants to blockade by intracellular spermine. (A) Macroscopic currents recorded in the presence of the indicated concentrations of spermine from excised patches of HEK293 T cells expressing WT Kir2.1 or the indicated mutant. Note the difference in the concentration ranges used for WT and mutants, as well as the difference in the time scales. K^+_o and K^+_i were 20 mM and 140 mM, respectively. The holding potential was −50 mV, and step pulses from +70 to −120 mV were applied in 10-mV decrements. (B) Normalized dose–block relationships; values were measured 800 ms (in WT and D259N) or 3,000 ms (in E224Q and E224Q/R228Q) after the onset of each step pulse. (C) Relationships between *K*d and voltage for spermine blockade of outward K^+ currents. Data obtained from three patches were plotted for each channel. The entire dataset could not be fitted with a straight line, but data from each patch was fitted with a straight line for the voltage range from −70 to −10 mV. (D) Relationships between voltage and the mean *K*d value in C. (E) Zd values of each channel calculated from the slopes of the lines in C. Mean values were compared statistically between WT and the mutants using Tukey's test (***, $P < 0.001$; *, $P < 0.05$; NS, $P > 0.05$); statistical comparison of the data obtained from E224Q and E224Q/R228Q is also shown. (F) Values of the Hill coefficient of each channel. Bars depict means ± SEM ($n = 3$). The symbols used are as indicated in the figure.

at depolarized potentials, even by 0.01 μM spermine. With E224Q, on the other hand, the slow blocking phase was not clearly observed, even with 1 μM spermine, but observed in the presence of 100 μM. Moreover, the blockade was almost completely eliminated by addition of a D259N mutation to E224Q. In the presence of 100 μM spermine, only a 7.4 ± 0.4% (n = 4) reduction in the amplitude in the outward current was observed at +70 mV, so that the analyses summarized in Fig. 6 could not be performed with E224Q/D259N. By contrast, with addition of an R228Q mutation to E224Q, outward currents were blocked by 0.1 μM spermine (Fig. 6).

The normalized steady-state dose–block relationships fitted with Hill's equation is shown in Fig. 6 B; *K*d values (n = 3) at each voltage and the lines fitted to them are shown in Fig. 6 C. The *K*d values all showed voltage dependence, the extent of which varied, but using all of the data, none could be fitted by a line due to the presence of extra conductances at highly depolarized potentials (Fig. 6 C). Two possible reported explanations for these extra conductances are (1) that spermine permeates through Kir2.1 at a highly depolarized potential (Guo and Lu, 2000a) and (2) that a second Kir2.1 form is present with a low *K*d for spermine blockade and a weak voltage dependence (Ishihara and Ehara, 2004). We did not try to clarify which of these models is correct, and, for the sake of convenience, the voltage dependences of spermine blockade were calculated by linear fitting of the data obtained at voltages ranging from −70 to −10 mV (Fig. 6 C). The mean *K*d values and zσ values are shown in Fig. 6 (D and E). The *K*d value for the spermine blockade of D259N at +40 mV was slightly larger than that for WT, and that for E224Q was much larger. The voltage dependence of the blockade of D259N was slightly weaker than in WT, and that in E224Q was much weaker. The diminished voltage dependency seen with E224Q was partially restored by addition of a R228Q mutation. Hill coefficients did not significantly correlate with voltage (Fig. 6 F).

Contribution of Charged Residues to the Single-channel Properties

Single-channel recordings were obtained from *Xenopus* oocytes using the cell-attached patch configuration in 140 mM K^+_o at −120 mV (Fig. 7 A); the traces on the left are shown on an expanded time scale to facilitate visualization of the fluctuations of the open-channel current. Mg^{2+} was removed from the pipette (extracellular) solution using EDTA in order to analyze the open-channel noise precisely. Also shown are the event histograms (Fig. 7 A, right) and the single-channel I-V relationships and the conductances (Fig. 7, B and C). Open-channel noise was increased with D259N, and clear subconducting states were seen (Fig. 7 A, arrows). With D259N, the single-channel substate conductance was smaller than the WT conductance, while that of the main component was similar to that of WT (Fig. 7 B). The incidence of the substate was ∼20–30% (confirmed in five patches). The single-channel conductance was much smaller with E224Q, and there was a substantial increase in open-channel noise associated with several subconducting states. It was difficult to discriminate the subconducting states precisely, so we plotted an average of the open-channel conductances (Fig. 7, B and C). We also observed that adding an R228Q mutation to E224Q partially restored the single-channel conductance and diminished the open-channel noise. The values of the single-channel conductances were 45.1 ± 0.7 pS (WT), 36.3 ± 1.3 pS (D259N-a; small component), 45.7 ± 1.5 pS (D259N-b; large component), 42.9 ± 0.8 pS (D259N; mean), 20.9 ± 1.4 pS (E224Q; mean), and 26.2 ± 0.7 pS (E224Q/R228Q), respectively (n = 3–4). The presence of a subconducting component suggests that K^+ permeation is unstable; i.e., energetically stable coordination of permeant K^+ within the selectivity filter may be reduced by the mutation.

Contribution of Charged Residues to Intrinsic Inward Rectification

The properties of Kir2.1 rectification are determined not only by cytoplasmic blockers but also by the characteristics of permeation in the absence of those blockers. For that reason, we next determined how the properties of the intrinsic rectification of the pore were affected by neutralization of the charged residues. Inward rectification in the absence of intracellular and extracellular blockers was analyzed using inside-out excised patch clamp recordings with a HEK293 cell expression system. For this analysis, step pulses from +100 to −100 mV were applied in 10-mV decrements, and two holding potentials were used: 0 and −100 mV. That the data obtained with the two holding potentials did not differ confirms the accuracy of the recordings. Representative macroscopic currents recorded using symmetrical 140 mM K^+ solutions and the mean normalized I-V relationships (n = 3–4) are shown in Fig. 8 (A and B). As an index of the intensity of the inward rectification, the ratios of the current amplitudes at +100 and −100 mV were calculated for each of the two holding potentials (Fig. 8 C). The intrinsic inward rectification of WT was weak, while that of D259N was slightly stronger than that of WT, and that of E224Q was much stronger. The intensity of the intrinsic rectification of E224Q was weakened by addition of an R228Q mutation. These results suggest that the intensity of intrinsic inward rectification was also controlled by the electrostatic circumstances within the cytoplasmic pore.

We also focused on the negatively charged amino acid residue E125, which is located within the extracellular loop of the channel protein (Fig. 10 A). Neutralization of E125 (E125N) was reported to reduce the susceptibility of the channel to blockade, the voltage dependence of the blockade by extracellular

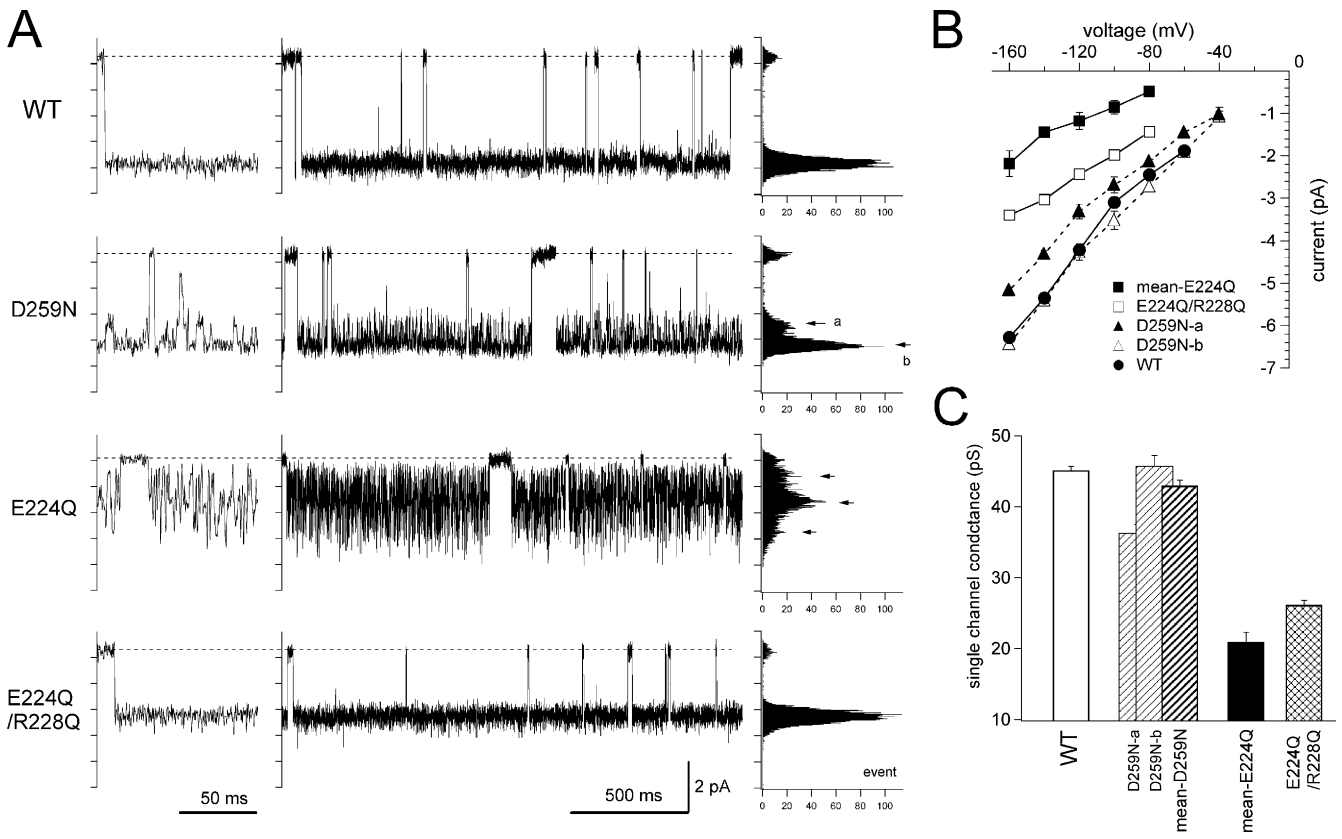

Figure 7. Comparison of single-channel currents through WT Kir2.1 and mutants. (A) Representative single-channel currents recorded from *Xenopus* oocytes using the cell-attached patch configuration. The K^+_o in the pipette and in the bath were 140 mM, and Mg^{2+} in the solution was chelated by EDTA. The holding potential was −120 mV. The dashed lines indicate the zero current level after subtracting the leak current. The traces are shown on an expanded time scale on the left, and event histograms are shown on the right. (B) Relationship between single-channel current amplitude and holding potential. Symbols are as shown in the figure. Bars depict means ± SEM (n = 3–4). (C) Single-channel conductance calculated from the slopes of the plots in B; plotted are means ± SEM (n = 3–4).

Ba^{2+} and Mg^{2+}, and the single channel conductance of K^+ permeation (Alagem et al., 2001; Murata et al., 2002). Based on those reports, we made E125Q and E125K mutants and analyzed their intrinsic rectification. Representative macroscopic currents and the mean I-V relationships are shown in Fig. 8 (D and E). The intrinsic inward rectification was weakened by the introduction of the E125Q mutation, and it was further weakened, rather outwardly rectified, by the E125K mutation. These changes caused by mutation of E125 were also observed in the presence of other background mutations (E224G and E224Q; unpublished data), which implies that E125 influences the intrinsic rectification from the extracellular side in a manner similar to the negative charges within the cytoplasmic pore.

Contribution of the Histidine Residue to Inward Rectification Properties

We next examined the functional significance of H226 located at the center of other charged residues (Fig. 1 C), whose electrostatic charge changes in accordance with the environmental pH (pKa value ∼6.0). This H226 residue was reported to contribute to the intracellular pH (pH_i)–sensitive flickery gating of the single channel in the E224G and E224A mutants (Xie et al., 2004). We made some H226 mutants and compared their inward rectification intensities with that of WT under the two-electrode voltage clamp (Fig. 9 A and Table I, group 8). H226K showed weaker inward rectification than WT, and a remarkable outward tail current was observed (Fig. 9 A). The macroscopic current of H226Q was mostly very small, and a recording with exceptionally high expression obtained by injecting ×20 concentrated cRNA to oocytes is shown in Fig. 9 A. Its rectification intensity was not different from that of WT (Fig. 9 A). The macroscopic currents of the H226A, R, E, and D mutants were also too small to be analyzed precisely. We next compared current through WT under pH_i 7.2 and pH_i 5.8 and the H226K mutant under pH_i 7.2, to know the contribution of a positive charge at position 226 (Fig. 9 B). An analysis of H226K under pH 5.8 could not be done because the current disappeared in all trials. The *K*d value for the $Mg^{2+}{}_i$ blockade of H226K (pH_i 7.2) at +70 mV was larger than that of WT (pH_i 7.2), and it was closer to that of WT (pH_i 5.8). The voltage dependence of the blockade of H226K (pH_i 7.2) was weaker

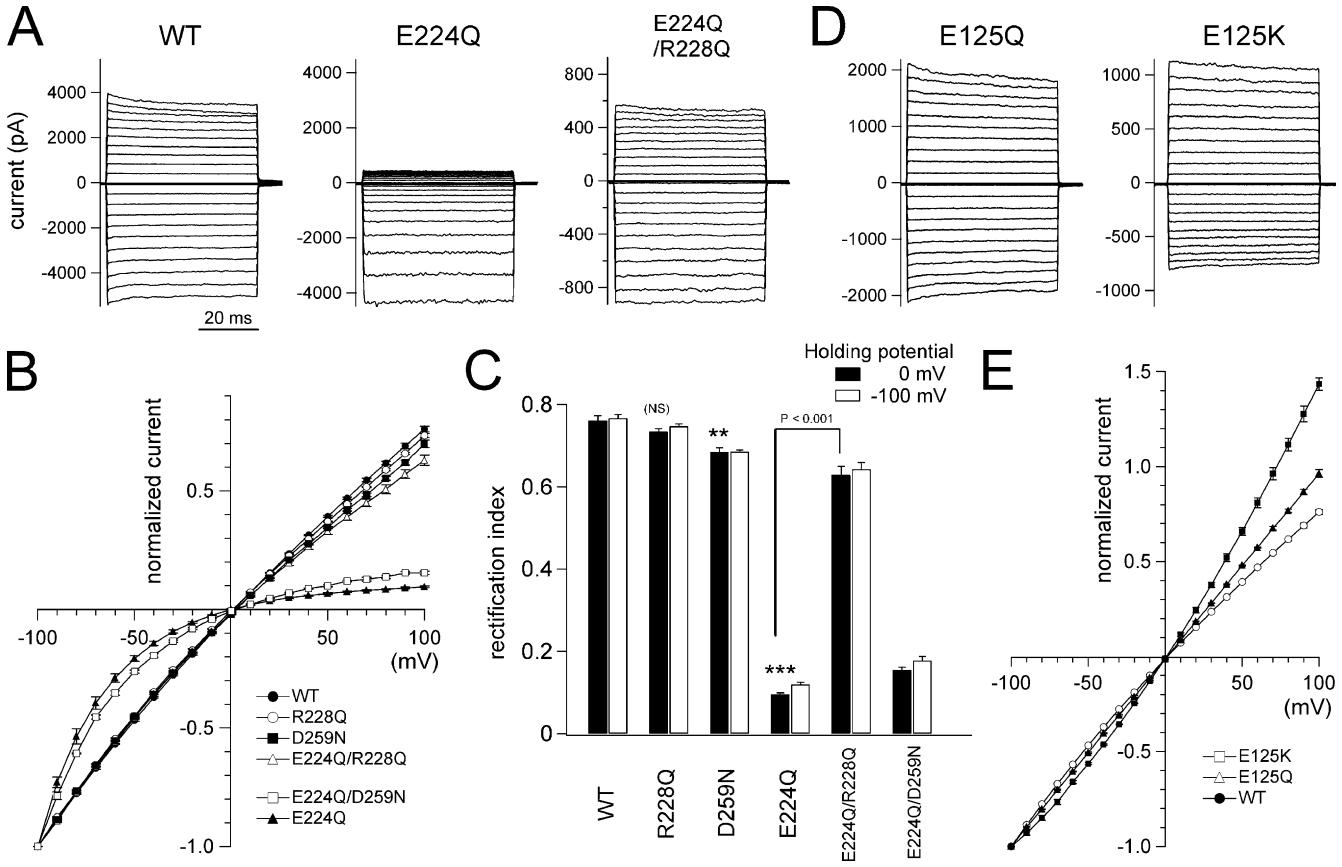

Figure 8. Comparison of the intrinsic inward rectification of WT Kir2.1 and the indicated mutants. (A) Macroscopic currents recorded in the absence of intracellular blockers from excised patches of HEK293T cells expressing WT or the indicated mutant. Representative current traces were recorded in solution containing 140 mM K^+ on both sides of the patch. The holding potential was 0 mV; step pulses from +100 to −100 mV were applied in 10-mV decrements. (B) Mean I-V relationships derived from the accumulated data; values were measured 2 ms after the onset of each step pulse. Bars depict means ± SEM (n = 3–4). The symbols used are as indicated in the figure. (C) The ratios of the current amplitudes measured 2 ms after the onset of step pulses to +100 and −100 mV were calculated as an index of rectification intensity. Two different holding potentials were used for recording and analysis: 0 mV (solid bars) and −100 mV (open bars). Bars depict means ± SEM (n = 3–4). Mean values were compared statistically between WT and the mutants using Tukey's test (***, $P < 0.001$; *, $P < 0.05$; NS, $P > 0.05$); statistical comparison of E224Q and E224Q/R228Q is also shown. (D and E) Contribution of the negatively charged amino acid residue at the outer mouth of the pore to the intrinsic inward rectification of Kir2.1. (D) Representative macroscopic currents through E125Q and E125K recorded as in A. (E) Mean I-V relationships analyzed as in B. Bars depict means ± SEM (n = 3–4). The symbols used are as indicated in the figure.

than that of WT (pH_i 7.2), and it was similar to that of WT (pH_i 5.8) (Fig. 9 B, right). We also analyzed the intrinsic inward rectification of WT and H226K from the identical patch. The intrinsic inward rectification of H226K (pH_i 7.2) was slightly stronger than that of WT (pH_i 7.2). The intrinsic inward rectification of WT became stronger with the decrease in pH_i (Fig. 9 C), and a decrease in the amplitude was also observed. The mean ± SEM values of the intrinsic inward rectification indexes and their statistical analyses using Tukey's test in WT were 0.78 ± 0.02 (pH_i 7.2, control) and 0.52 ± 0.03 (pH_i 5.8, $P < 0.001$), and the values in H226K were 0.65 ± 0.02 (under pH_i 7.2, $P < 0.05$), respectively (n = 4). As the values in H226K under pH_i 6.6 showed a slight but nonsignificant decrease (0.56 ± 0.03, $P > 0.05$ (in comparison with H226K [pH_i 7.2], n = 4), it seems the effect of pH_i on intrinsic rectification is mediated also by mechanisms other than the protonation at 226. In summary, a positive charge at 226 provided by H226K mutation or by intr acellular acidification of WT was shown to weaken inward rectification, to decrease the sensitivity to the block by $Mg^{2+}{}_i$, and to increase intrinsic inward rectification in the absence of blockers. These data show that a positive charge at 226 also plays significant roles as other charged amino acid residues do.

DISCUSSION

Correlation of Location of Charged Amino Acids and their Contribution to Channel Properties

We observed that mutations that neutralized the negative charges on the wall of the cytoplasmic pore

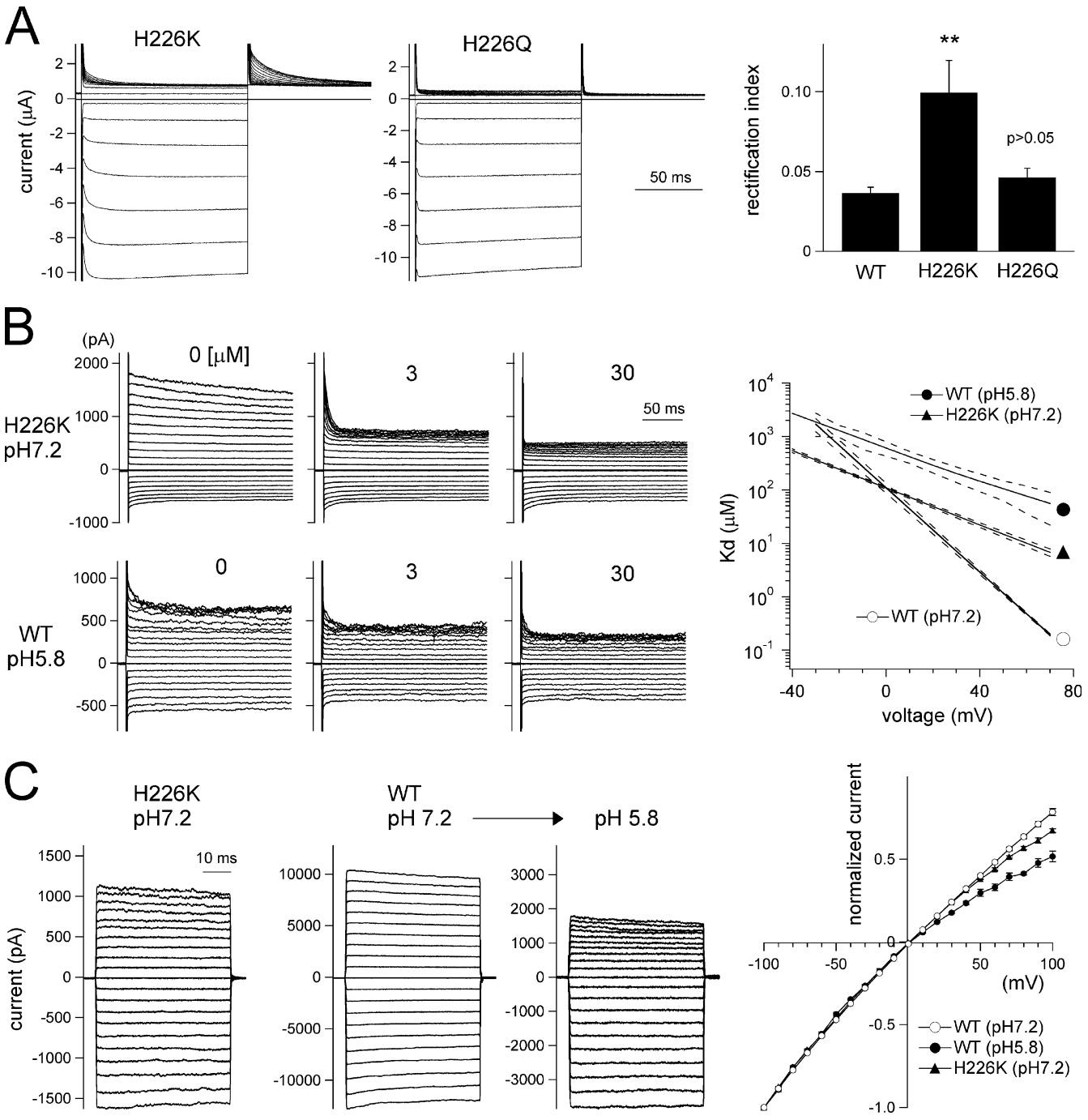

Figure 9. Comparison of the inward rectification properties of macroscopic currents through WT Kir2.1 and the indicated mutants of the H226 residue. (A) Macroscopic currents recorded using two-electrode voltage clamp with *Xenopus* oocytes and the intensities of the inward rectification of them were analyzed as in Fig 2. Bars depict means ± SEM (n = 4–5), and the values were compared statistically between WT and the mutants using Tukey's test (**, $P < 0.01$; $P > 0.05$). (B) Comparison of the susceptibility of macroscopic currents through WT Kir2.1 and H226K under the indicated intracellular pH to blockade by intracellular Mg^{2+}. Macroscopic currents recorded in the presence of the indicated concentrations of Mg^{2+}_i from excised patches of HEK293T cells as in Fig. 5. The concentrations of Mg^{2+}_i are shown in the figure. The relationships between the *K*d and voltage for Mg^{2+}_i blockade of outward K^+ currents are shown on the right. The solid lines with symbols indicate the means of the fitted lines with data obtained from four patches for H226K (pH 7.2) and WT (pH 5.8), and the dashed lines indicate SEMs. For reference, the data of WT (pH 7.2) shown in Fig. 5 were also plotted with SEM. (C) Comparison of the intrinsic inward rectification of WT and H226K as in Fig. 8. Bars depict means ± SEM (n = 4) of the normalized current at each voltage. The symbols used are as indicated in the figure.

(E224Q, E299Q, and D259N) reduced the intensity of inward rectification and slowed the activation of inward currents and the decay of outward currents, and that additional mutations neutralizing the positive charges (R228Q and R260Q) had the opposite effect. We also observed protonation at H226 by intracellular acidification or the H226K mutation changed these channel properties. It thus appears that increases in the net negativity within the cytoplasmic pore tends to enhance inward rectification properties (Figs. 2–4, Fig. 9, and Tables I and II), which is consistent with the interpretation proposed by Pegan et al. (2005).

As a next step, we selected several point mutants that reflect this tendency and, using inside-out patch clamp recordings, systematically analyzed the contributions of the affected residues to the blockade by intracellular blockers and to K^+ permeation (Figs. 5–9). The analyzed parameters were all influenced by the electrostatic negativity within the cytoplasmic pore. With a decrease in the number of negative charges, (1) *K*d values for both the $Mg^{2+}{}_i$ and spermine blockades were increased, (2) the voltage dependencies were reduced, (3) the single-channel conductance was reduced, (4) open-channel noise was increased, and (5) intrinsic inward rectification was enhanced. These values were partially restored by additional neutralization of a positive charge. Thus, both channel blockade and K^+ permeation were influenced by the net charge within the cytoplasmic pore.

In all of our analyses, the magnitudes of the changes caused by D259N mutation were substantially milder than those caused by E224Q mutation. For instance, the magnitude of the effect of mutation on inward rectification was very large with E224Q, moderate with E299Q and D259N, and small with D255N (Table I, groups 1 and 2). Moreover, addition of either R228Q or R260Q mutation to E224Q significantly shifted the parameters toward WT values in all analyses, and the magnitudes of their effects were similar. The contributions of these charges can be explained by their location within the cytoplasmic pore (Fig. 10 A). With the channel oriented as in Fig. 10 A, a negatively charged ring composed of E224 and E299 is located at the top of the cytoplasmic pore, and an E224 ring is located inside of the E299 ring. A negatively charged ring composed of D259 is located below them, within the cytoplasmic pore, and D255 much farther below. Two positively charged rings composed of R228 and R260 overlap one another and are located between the E224 and D259 rings. One would expect that charged amino acids located near the mouth of the transmembrane pore would make larger contributions to inward rectification, even though the width of the cytoplasmic pore is nearly constant. Thus, the locations of the charged amino acids correlated well with the magnitudes of their contributions to the inward rectification.

Contribution of the Charged Amino Acids in Concentrating K^+ within the Cytoplasmic Pore

We observed that the reduction of the net negative charge within the cytoplasmic pore increased the incidence of flickering subconducting states, which resulted in an increase in the open-channel noise and a decrease in the single-channel conductance. A possible interpretation about the arising of the subconducting states was proposed by Xie et al. (2004). They assumed the subconductance was caused by a fast gating, and K^+ flux through Kir2.1 is regulated by the gate trapping spermine located at bundle crossing or below. This interpretation is based on the observation that spermine unblock is markedly slowed in E224Q, suggesting that the subconducting states may be trapping spermine in the pore (Xie et al., 2004). Another interpretation has also been proposed that the subconductance is derived from the lack of K^+ in the selectivity filter. Lu et al. (2001) analyzed the single channel properties of Kir2.1 by introducing backbone mutations into the selectivity filter. They suggested that the subconducting states resulted from the collapse of the ion–ion interacting permeation, which was caused by the lack of specific K^+ coordination within the selectivity filter (Lu et al., 2001). In addition, symmetric increases in $[K^+]$ on both sides of the channel enhance the main-state probability (Chang et al., 2005), suggesting that for efficient permeation, it is necessary to have the selectivity filter filled with permeating K^+. In that regard, the cytoplasmic negative charge may play a role in elevating the local concentration of K^+ in the transmembrane permeation pathway by attracting K^+ in the cytoplasmic vestibule, thereby supporting permeation through the selectivity filter. This interpretation may also explain the effect of neutralizing mutations on the intrinsic inward rectification, which is possibly due to saturation of the outward flux of K^+ ions through the pore. Saturation of the ion flux was also reported for permeation through the gramicidin channel when the concentration of charge carrier was low (Andersen, 1984; Koeppe and Anderson, 1996), as well as in the BK channel in the absence of negative charges located on the transmembrane inner vestibule (Brelidze et al., 2003; Brelidze and Magleby, 2005). When neutralized, the cytoplasmic pore could be an obstacle to the entry of K^+ into the permeation pathway, so that resistance within the pore, rather than the K^+ flux through the selectivity filter, might become the rate-limiting step for K^+ efflux. We therefore propose that the negative electrostatic potential within the cytoplasmic pore plays a key role in increasing the local concentration of K^+ to supply sufficient K^+ ions to the transmembrane region, which in turn enables smooth permeation of fully coordinated K^+ ions within the selectivity filter. Considering the electrostatic effect of the charged amino acid at E125 at the extracellular mouth (Fig. 8, D and E), we also speculate that the valance of K^+ ions pooled on the

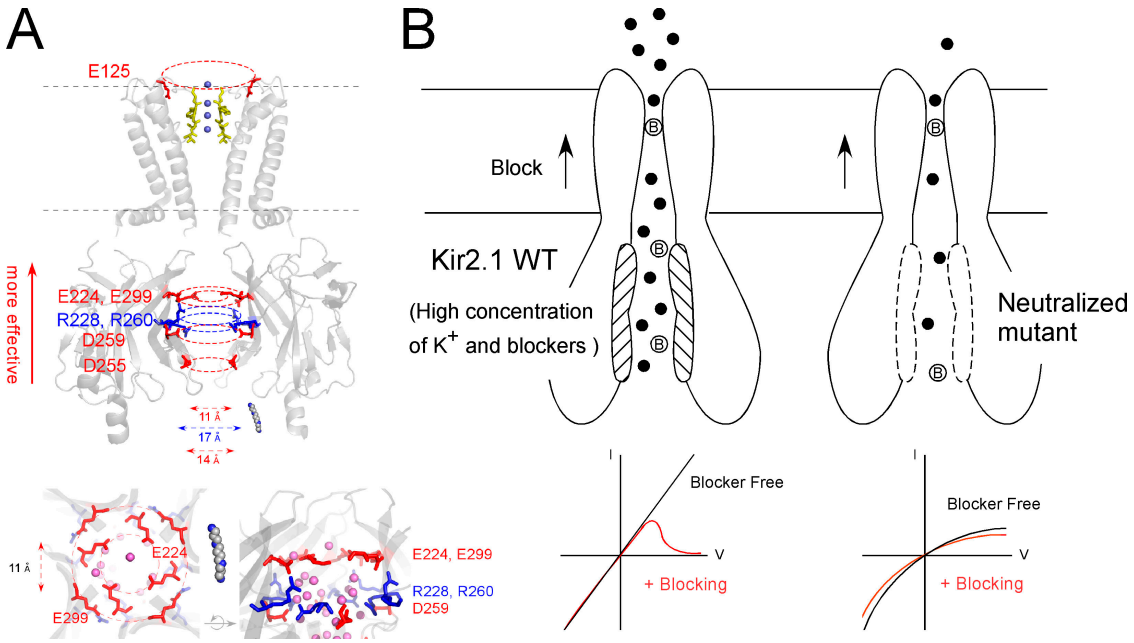

Figure 10. Schematic drawings illustrating the mechanism of the voltage-dependent blockade of Kir2.1. (A) Model of the long pore of the permeation pathway based on the structures of Kir2.1 and KirBac1.1. Negatively and positively charged amino acid residues are respectively indicated with red and blue sticks; the selectivity filter is indicated with yellow sticks. K^+ ions and a spermine are indicated with space fillings. Dotted circles depict the charged rings with the diameters shown. (B) Schematic drawings explaining the function of the cytoplasmic pore in WT Kir2.1 (left) and a neutralized mutant (right). The filled circles indicate K^+ ions, and the Bs indicate blocker molecules. On the left, the negatively charged cytoplasmic pore (obliquely lined) electrostatically gathers cations, such as K^+ and blockers, and as a result the blocking area in the transmembrane are smoothly furnished with many K^+, enabling high affinity, strongly voltage-dependent blockade with adequate outward K^+ conductance. The bottom drawings illustrate the I-V relationships with and without the blockers in WT Kir2.1 and a neutralized mutant. With the WT channel, in which the negativity of the pore is intact, the outward current is steeply blocked with a significant K^+ efflux at membrane potentials slightly above E_K. This characteristic may facilitate generation of the cardiac action potential.

each side of the GYG selectivity filter may determine the intrinsic rectification intensity.

The Cytoplasmic Pore Is Not the Final Plugging Site for the Blockers

In this and our earlier study (Kubo and Murata, 2001), we analyzed the speed of hyperpolarization-evoked activation (i.e., off-blocking) in various mutants. We found that activation tended to slow down with a reduction in the net negative charges within the cytoplasmic pore. These results were in clear contrast with the observation in the transmembrane D172N mutation, in which activation became almost instantaneous (Lu and MacKinnon, 1994; Stanfield et al., 1994; Wible et al., 1994). If intracellular blockers ultimately plug channel at the cytoplasmic pore, the off-blocking rate would be expected to be increased by neutralization of the negative charges; i.e., hyperpolarization-evoked activation would be faster not slower (Kubo and Murata, 2001). This makes it unlikely that the cytoplasmic pore is the site at which blockers bind and plug the channel. We speculate that electrostatic negativity in the cytoplasmic pore facilitates off-blocking of spermine from the final plugging site by attracting spermine to the cytoplasmic pore at hyperpolarized potentials. There have been several reports suggesting that intracellular blockers plug the channel at deeper sites (D172 and S165), near the selectivity filter, using mutagenesis study or cationic cys-modifying reagents (Lu and MacKinnon, 1994; Stanfield et al., 1994; Wible et al., 1994; Lu et al., 1999; Fujiwara and Kubo, 2002; Chang et al., 2003). In the resolved crystal structure of Kir2.1, the vacancy created by the cytoplasmic pore is large enough to hold 25 water molecules ($\sim 17 \times 17 \times 30$ Å), far too large for the blocker molecules to stably plug the channel and stop the K^+ flux at that point in the permeation pathway (Fig. 10 A). We therefore propose that the final plugging site is not within the cytoplasmic pore, but that the cytoplasmic pore nevertheless affects the permeation of both intracellular blockers and K^+ through it.

Strong Voltage Dependence of the Blockade

Voltage dependence reflects the movement of charged particles across an electric field. Charge movements through the electric field within Kir channels are reportedly caused mainly by movements of permeant K^+ ions pushed by the blockers during the blocking process rather than the movement of the blockers themselves (Oliver et al., 1998; Pearson and Nichols, 1998; Spassova

and Lu, 1998). In the present study, we observed clear changes in the voltage dependence of the blockade with neutralization of charges on the surface of the cytoplasmic pore even using Mg^{2+}, which is very unlikely to occlude permeation at the wide cytoplasmic pore. So if the final plugging site(s) for intracellular blockers was unaltered by the mutations within the cytoplasmic pore, why did the voltage dependence of block change so much?

With the assumption that the blockade occurred within the transmembrane region of the permeation pathway, beyond the cytoplasmic pore, we suggest so far that the negativity within the cytoplasmic pore electrostatically concentrates not only blockers but also K^+, so that there is sufficient K^+ to be smoothly coordinated within the transmembrane pore (Fig. 10 B, left). During the blocking process, blockers can push out more K^+ ions from the electric field, so that a more voltage-dependent block would arise (Fig. 10 B, left). That neutralization of the negative charge within the cytoplasmic pore reduced the voltage dependence of the blockade can thus be explained by a reduction in the ability to concentrate K^+ ions (Fig. 10 B, right). We think this K^+-based explanation is compatible with various observations made with Kir2.1 and also with Kir6.2 (Kurata et al., 2004), but we have no conclusive structural information about the coordination sites of K^+ or intracellular blockers within the transmembrane and/or cytoplasmic pore. There is also a possibility that long-range effects in protein (Bichet et al., 2004; Gazzarrini et al., 2004) due to the cytoplasmic mutations may influence the transmembrane structure. The transmembrane structure of Kir2.1 is thought to be different from KcsA (Minor et al., 1999; Chatelain et al., 2005), so its crystal analysis will be needed to fully clarify the inward rectification mechanism in Kir2.1.

We are grateful to Dr. J. Miyazaki (Osaka University, Osaka, Japan) for providing us with pCXN2 expression vector. We would like to thank members of the Kubo laboratory (National Institute for Physiological Sciences) for helpful discussions and Ms. Y. Asai for technical assistance.

This work was supported in part by research grants from the Ministry of Education, Science, Sports, Culture, and Technology of Japan and from the Japan Society for Promotion of Science to Y. Kubo, and by a research fellowship from the Japan Society for Promotion of Science for Young Scientists to Y. Fujiwara.

Lawrence G. Palmer served as editor.

Submitted: 14 October 2005
Accepted: 15 February 2006

REFERENCES

Alagem, N., M. Dvir, and E. Reuveny. 2001. Mechanism of Ba^{2+} block of a mouse inwardly rectifying K^+ channel: differential contribution by two discrete residues. *J. Physiol.* 534:381–393.

Andersen, O.S. 1984. Gramicidin channels. *Annu. Rev. Physiol.* 46:531–548.

Bichet, D., Y.F. Lin, C.A. Ibarra, C.S. Huang, B.A. Yi, Y.N. Jan, and L.Y. Jan. 2004. Evolving potassium channels by means of yeast selection reveals structural elements important for selectivity. *Proc. Natl. Acad. Sci. USA.* 101:4441–4446.

Bond, C.T., M. Pessia, X.M. Xia, A. Lagrutta, M.P. Kavanaugh, and J.P. Adelman. 1994. Cloning and expression of a family of inward rectifier potassium channels. *Receptors Channels.* 2:183–191.

Brelidze, T.I., and K.L. Magleby. 2005. Probing the geometry of the inner vestibule of BK channels with sugars. *J. Gen. Physiol.* 126:105–121.

Brelidze, T.I., X. Niu, and K.L. Magleby. 2003. A ring of eight conserved negatively charged amino acids doubles the conductance of BK channels and prevents inward rectification. *Proc. Natl. Acad. Sci. USA.* 100:9017–9022.

Chang, H.K., S.H. Yeh, and R.C. Shieh. 2003. The effects of spermine on the accessibility of residues in the M2 segment of Kir2.1 channels expressed in *Xenopus* oocytes. *J. Physiol.* 553:101–112.

Chang, H.K., S.H. Yeh, and R.C. Shieh. 2005. A ring of negative charges in the intracellular vestibule of Kir2.1 channel modulates K^+ permeation. *Biophys. J.* 88:243–254.

Chatelain, F.C., N. Alagem, Q. Xu, R. Pancaroglu, E. Reuveny, and D.L. Minor Jr. 2005. The pore helix dipole has a minor role in inward rectifier channel function. *Neuron.* 47:833–843.

Fakler, B., U. Brandle, E. Glowatzki, S. Weidemann, H.P. Zenner, and J.P. Ruppersberg. 1995. Strong voltage-dependent inward rectification of inward rectifier K^+ channels is caused by intracellular spermine. *Cell.* 80:149–154.

Ficker, E., M. Taglialatela, B.A. Wible, C.M. Henley, and A.M. Brown. 1994. Spermine and spermidine as gating molecules for inward rectifier K^+ channels. *Science.* 266:1068–1072.

Fujiwara, Y., and Y. Kubo. 2002. Ser165 in the second transmembrane region of the Kir2.1 channel determines its susceptibility to blockade by intracellular Mg^{2+}. *J. Gen. Physiol.* 120:677–693.

Gazzarrini, S., M. Kang, J.L. Van Etten, S. Tayefeh, S.M. Kast, D. DiFrancesco, G. Thiel, and A. Moroni. 2004. Long distance interactions within the potassium channel pore are revealed by molecular diversity of viral proteins. *J. Biol. Chem.* 279:28443–28449.

Guo, D., and Z. Lu. 2000a. Mechanism of IRK1 channel block by intracellular polyamines. *J. Gen. Physiol.* 115:799–814.

Guo, D., and Z. Lu. 2000b. Pore block versus intrinsic gating in the mechanism of inward rectification in strongly rectifying IRK1 channels. *J. Gen. Physiol.* 116:561–568.

Guo, D., and Z. Lu. 2002. IRK1 inward rectifier K^+ channels exhibit no intrinsic rectification. *J. Gen. Physiol.* 120:539–551.

Guo, D., and Z. Lu. 2003. Interaction mechanisms between polyamines and IRK1 inward rectifier K^+ channels. *J. Gen. Physiol.* 122:485–500.

Hagiwara, S., and K. Takahashi. 1974. The anomalous rectification and cation selectivity of the membrane of a starfish egg cell. *J. Membr. Biol.* 18:61–80.

Hagiwara, S., and M. Yoshii. 1979. Effects of internal potassium and sodium on the anomalous rectification of the starfish egg as examined by internal perfusion. *J. Physiol.* 292:251–265.

Hille, B. 2001. Ion Channels of Excitable Membranes. Third edition. Sinauer Associates Inc., Sunderland, MA. 506 pp.

Ho, K., C.G. Nichols, W.J. Lederer, J. Lytton, P.M. Vassilev, M.V. Kanazirska, and S.C. Hebert. 1993. Cloning and expression of an inwardly rectifying ATP-regulated potassium channel. *Nature.* 362:31–38.

Inagaki, N., T. Gonoi, J.P. Clement IV, N. Namba, J. Inazawa, G. Gonzalez, L. Aguilar-Bryan, S. Seino, and J. Bryan. 1995. Reconstitution of IKATP: an inward rectifier subunit plus the sulfonylurea receptor. *Science.* 270:1166–1170.

Ishihara, K., and T. Ehara. 2004. Two modes of polyamine block regulating the cardiac inward rectifier K^+ current IK1 as revealed by a study of the Kir2.1 channel expressed in a human cell line. *J. Physiol.* 556:61–78.

Ishihara, K., M. Hiraoka, and R. Ochi. 1996. The tetravalent organic cation spermine causes the gating of the IRK1 channel expressed in murine fibroblast cells. *J. Physiol.* 491:367–381.

Koeppe, R.E., II, and O.S. Anderson. 1996. Engineering the gramicidin channel. *Annu. Rev. Biophys. Biomol. Struct.* 25:231–258.

Kubo, Y., T.J. Baldwin, Y.N. Jan, and L.Y. Jan. 1993a. Primary structure and functional expression of a mouse inward rectifier potassium channel. *Nature.* 362:127–133.

Kubo, Y., and Y. Murata. 2001. Control of rectification and permeation by two distinct sites after the second transmembrane region in Kir2.1 K^+ channel. *J. Physiol.* 531:645–660.

Kubo, Y., E. Reuveny, P.A. Slesinger, Y.N. Jan, and L.Y. Jan. 1993b. Primary structure and functional expression of a rat G-protein-coupled muscarinic potassium channel. *Nature.* 364:802–806.

Kuo, A., J.M. Gulbis, J.F. Antcliff, T. Rahman, E.D. Lowe, J. Zimmer, J. Cuthbertson, F.M. Ashcroft, T. Ezaki, and D.A. Doyle. 2003. Crystal structure of the potassium channel KirBac1.1 in the closed state. *Science.* 300:1922–1926.

Kurata, H.T., L.R. Phillips, T. Rose, G. Loussouarn, S. Herlitze, H. Fritzenschaft, D. Enkvetchakul, C.G. Nichols, and T. Baukrowitz. 2004. Molecular basis of inward rectification: polyamine interaction sites located by combined channel and ligand mutagenesis. *J. Gen. Physiol.* 124:541–554.

Lopatin, A.N., E.N. Makhina, and C.G. Nichols. 1994. Potassium channel block by cytoplasmic polyamines as the mechanism of intrinsic rectification. *Nature.* 372:366–369.

Lu, T., B. Nguyen, X. Zhang, and J. Yang. 1999. Architecture of a K^+ channel inner pore revealed by stoichiometric covalent modification. *Neuron.* 22:571–580.

Lu, T., L. Wu, J. Xiao, and J. Yang. 2001. Permeant ion-dependent changes in gating of Kir2.1 inward rectifier potassium channels. *J. Gen. Physiol.* 118:509–522.

Lu, Z., and R. MacKinnon. 1994. Electrostatic tuning of Mg^{2+} affinity in an inward-rectifier K^+ channel. *Nature.* 371:243–246.

Luo, C.H., and Y. Rudy. 1994. A dynamic model of the cardiac ventricular action potential. I. Simulations of ionic currents and concentration changes. *Circ. Res.* 74:1071–1096.

Ma, D., N. Zerangue, Y.F. Lin, A. Collins, M. Yu, Y.N. Jan, and L.Y. Jan. 2001. Role of ER export signals in controlling surface potassium channel numbers. *Science.* 291:316–319.

Matsuda, H. 1988. Open-state substructure of inwardly rectifying potassium channels revealed by magnesium block in guinea-pig heart cells. *J. Physiol.* 397:237–258.

Matsuda, H., A. Saigusa, and H. Irisawa. 1987. Ohmic conductance through the inwardly rectifying K channel and blocking by internal Mg^{2+}. *Nature.* 325:156–159.

Matsuoka, S., N. Sarai, S. Kuratomi, K. Ono, and A. Noma. 2003. Role of individual ionic current systems in ventricular cells hypothesized by a model study. *Jpn. J. Physiol.* 53:105–123.

Minor, D.L., Jr., S.J. Masseling, Y.N. Jan, and L.Y. Jan. 1999. Transmembrane structure of an inwardly rectifying potassium channel. *Cell.* 96:879–891.

Murata, Y., Y. Fujiwara, and Y. Kubo. 2002. Identification of a site involved in the block by extracellular Mg^{2+} and Ba^{2+} as well as permeation of K^+ in the Kir2.1 K^+ channel. *J. Physiol.* 544:665–677.

Nichols, C.G., and A.N. Lopatin. 1997. Inward rectifier potassium channels. *Annu. Rev. Physiol.* 59:171–191.

Nishida, M., and R. MacKinnon. 2002. Structural basis of inward rectification: cytoplasmic pore of the G protein-gated inward rectifier GIRK1 at 1.8 Å resolution. *Cell.* 111:957–965.

Niwa, H., K. Yamamura, and J. Miyazaki. 1991. Efficient selection for high-expression transfectants with a novel eukaryotic vector. *Gene.* 108:193–199.

Oliver, D., H. Hahn, C. Antz, J.P. Ruppersberg, and B. Fakler. 1998. Interaction of permeant and blocking ions in cloned inward-rectifier K^+ channels. *Biophys. J.* 74:2318–2326.

Pearson, W.L., and C.G. Nichols. 1998. Block of the Kir2.1 channel pore by alkylamine analogues of endogenous polyamines. *J. Gen. Physiol.* 112:351–363.

Pegan, S., C. Arrabit, W. Zhou, W. Kwiatkowski, A. Collins, P.A. Slesinger, and S. Choe. 2005. Cytoplasmic domain structures of Kir2.1 and Kir3.1 show sites for modulating gating and rectification. *Nat. Neurosci.* 8:279–287.

Sabirov, R.Z., T. Tominaga, A. Miwa, Y. Okada, and S. Oiki. 1997. A conserved arginine residue in the pore region of an inward rectifier K channel (IRK1) as an external barrier for cationic blockers. *J. Gen. Physiol.* 110:665–677.

Spassova, M., and Z. Lu. 1998. Coupled ion movement underlies rectification in an inward-rectifier K^+ channel. *J. Gen. Physiol.* 112:211–221.

Stanfield, P.R., N.W. Davies, P.A. Shelton, M.J. Sutcliffe, I.A. Khan, W.J. Brammar, and E.C. Conley. 1994. A single aspartate residue is involved in both intrinsic gating and blockage by Mg^{2+} of the inward rectifier, IRK1. *J. Physiol.* 478:1–6.

Stockklausner, C., J. Ludwig, J.P. Ruppersberg, and N. Klocker. 2001. A sequence motif responsible for ER export and surface expression of Kir2.0 inward rectifier K^+ channels. *FEBS Lett.* 493:129–133.

Taglialatela, M., E. Ficker, B.A. Wible, and A.M. Brown. 1995. C-terminus determinants for Mg^{2+} and polyamine block of the inward rectifier K^+ channel IRK1. *EMBO J.* 14:5532–5541.

Takumi, T., T. Ishii, Y. Horio, K. Morishige, N. Takahashi, M. Yamada, T. Yamashita, H. Kiyama, K. Sohmiya, S. Nakanishi, et al. 1995. A novel ATP-dependent inward rectifier potassium channel expressed predominantly in glial cells. *J. Biol. Chem.* 270:16339–16346.

Vandenberg, C.A. 1987. Inward rectification of a potassium channel in cardiac ventricular cells depends on internal magnesium ions. *Proc. Natl. Acad. Sci. USA.* 84:2560–2564.

Wible, B.A., M. Taglialatela, E. Ficker, and A.M. Brown. 1994. Gating of inwardly rectifying K^+ channels localized to a single negatively charged residue. *Nature.* 371:246–249.

Xie, L.H., S.A. John, and J.N. Weiss. 2002. Spermine block of the strong inward rectifier potassium channel Kir2.1: dual roles of surface charge screening and pore block. *J. Gen. Physiol.* 120:53–66.

Xie, L.H., S.A. John, and J.N. Weiss. 2003. Inward rectification by polyamines in mouse Kir2.1 channels: synergy between blocking components. *J. Physiol.* 550:67–82.

Xie, L.H., S.A. John, B. Ribalet, and J.N. Weiss. 2004. Regulation of gating by negative charges in the cytoplasmic pore in the Kir2.1 channel. *J. Physiol.* 561:159–168.

Yang, J., Y.N. Jan, and L.Y. Jan. 1995. Control of rectification and permeation by residues in two distinct domains in an inward rectifier K^+ channel. *Neuron.* 14:1047–1054.